Atmospheric Pollutant Levels in Southeast Brazil During COVID-19 Lockdown: Combined Satellite and Ground-based Data Analysis

Rayssa Brandao

Thesis submitted to the faculty of the Virginia Polytechnic Institute and State University in partial fulfillment of the requirements for the degree of

Master of Science
In
Environmental Engineering

Hosein Foroutan, Chair
Linsey C. Marr
Elena S. Lind

December 17, 2020
Blacksburg, VA

Keywords: air pollution, satellite, surface air quality, COVID-19, lockdown, Brazil

Atmospheric Pollutant Levels in Southeast Brazil During COVID-19 Lockdown: Combined Satellite and Ground-based Data Analysis

Rayssa Brandao

ABSTRACT

With the ongoing COVID-19 pandemic being spread all over the world, lockdown measures are being implemented making air pollution levels go down in several countries. In this context, the air quality changes in the highly populated and trafficked Brazilian states of Sao Paulo (SP) and Rio de Janeiro (RJ) are hereby going to be addressed using a combination of satellite and ground-based data analysis. We explored nitrogen dioxide (NO_2) and particulate matter ($PM_{2.5}$) daily levels for the month of May during different years within 2015-2020. Daily measurements of NO_2 column concentrations from the Ozone Monitoring Instrument (OMI) aboard NASA's Aura satellite were also gathered and averaged decreases of 42% and 49.6% were found for the year of 2020 compared to previous averaged 2015-2019 years. In parallel to the NO_2 column retrieval, the ground-based data, measured by the Brazilian States Environmental Institutions, is analyzed, and correlated with satellite retrievals. Correlation coefficients between column and ground-based concentrations were 77% and 53% in SP and RJ, respectively. It was found a 13.3% (p-value = 0.099) and 18.8% (p-value = 0.077) decrease in NO_2 levels for SP and RJ, respectively, in 2020 compared to 2019. For $PM_{2.5}$, no significant change was observed for the same time period in the SP region, although the high number of fire burnings in the Southeast region seemed to be affecting $PM_{2.5}$ levels. In addition to natural emissions (fire burnings), the combined data was also evaluated taking meteorological parameters, such as temperature and wind speed, into account. No interference of weather or fire was found in 2020 NO_2 ground levels compared to previous years, This integrated analysis is innovative and has yet to be more explored in Brazilian studies. This is true specifically because the ground-based stations are spatially and temporally sparse in Brazil.

Atmospheric Pollutant Levels in Southeast Brazil During COVID-19 Lockdown: Combined Satellite and Ground-based Data Analysis

Rayssa Brandao

GENERAL AUDIENCE ABSTRACT

This study aims to explore satellite data applied to the lockdown context resultant from the COVID-19 pandemic in Brazil. Satellite data usage in air quality management is yet to be explored to its full potential. Two highly populated states were chosen: Sao Paulo (SP) and Rio de Janeiro (RJ). Local governments have been imposing limitations on private and public vehicle circulation, inducing a decrease in atmospheric pollutant levels, specifically nitrogen dioxide (NO_2), which is directly emitted to the air by fuel combustion. NO_2 is also short-lived in the atmosphere, so its variation within days can be easily captured. $PM_{2.5}$, a category of fine inhalable particles, can be produced by wildfires, in addition to fuel burning and mechanical processes such as resuspension by cars. Here we retrieved daily NO_2 vertical column densities for the month of May within the 2015-2020 years from the OMI instrument onboard of NASA's Aura satellite. Ground daily NO_2 and $PM_{2.5}$ measurements were also collected from local environmental agencies. Results showed an average 42% decrease of the NO_2 column values in SP in 2020 compared to 2015-2019. The decrease was 49.6% in RJ for the same timeframe. Correspondent surface data showed a decrease of 13.3% (p-value = 0.099) and 18.8% (p-value = 0.077) during 2020 compared to 2019 in SP and RJ stations, respectively. No significant divergence in $PM_{2.5}$ values was found between 2019 and 2020. Finally, weather data was added to the pollutant analysis. $PM_{2.5}$ concentrations were associated with wildfires, while the NO_2 levels found in 2020 for SP and RJ were attributed to local lockdown decrees. Satellite retrievals showed significant potential in filling out ground datasets, correlating with the SP and RJ surface data in 77% and 53%, respectively.

TABLE OF CONTENTS

List of Figures v
List of Tables vi
Chapter 1. Introduction 1
1.1 Overview 1
1.2 Background 1
1.2.1 Satellites 1
1.2.1.1 Definition 2
1.2.1.2 Capabilities and Characteristics 2
1.2.1.3 Satellite systems orbits 3
1.2.1.4 Satellite systems examples 4
1.2.2 Satellite Systems Instruments 4
1.2.2.1 Electromagnetic Energy 5
1.2.2.2 Instrument Categorization 7
1.2.3 Instrument Data Products 8
1.2.3.1 Product Level Classification 8
1.2.3.2 Relevant Data Variables 9
1.2.4 $OMNO_2$ retrieval algorithm 9
1.2.4.1 SP2 Summary 10
1.2.4.2 Sources of Error 11
1.2.4.3 Satellite Retrieval Differences from Aircraft, Ground and Modeled NO_2 12
1.2.4.4 Version 3.0 $OMNO_2$ Data Product Improvements 13
1.2.5 Review of Applied Satellite Data in Literature 14
1.3 Objectives 15
References 16
Chapter 2. Atmospheric pollutant levels in Southeast Brazil during COVID-19 lockdown: combined satellite and ground-based data analysis 20
2.1 Abstract 21
2.2 Introduction 22
2.3 Materials and Methods 27
2.3.1 Satellite Retrievals of Tropospheric NO2 27
2.3.2 Satellite Data Analysis 28
2.3.3 Ground-Level Measurements 29
2.3.4 Temporal Correlation Analysis 32
2.4 Results and Discussion 33
2.4.1 Qualitative Plots 33
2.4.2 Quantitative Analysis 34
2.4.2.1 OMNO2d Satellite Retrievals 34
2.4.2.2 Ground-based Analysis 35
2.4.2.3 Correlation Analysis 40
2.4.3 Meteorological Conditions and Natural Emissions 42
2.4.4 Data Limitations 47
2.5 Conclusions 48
2.6 Acknowledgments 50
References 50
Chapter 3. Conclusion 56
3.1 Conclusions 56
3.2 Recommendations for Future Work 58
Appendix A. ADDITIONAL SATELLITE SYSTEMS INFORMATION 60
Appendix B. ADDITIONAL SATELLITE INSTRUMENTS INFORMATION 62

List of Figures

Figure 1. Electromagnetic wave……...5

Figure 2. Wave characteristics……..…6

Figure 3. Electromagnetic Spectrum……....6

Figure 4. Selected Brazil states (SP and RJ) and their hydrographic regions……...…….……....26

Figure 5. The six selected ground stations in SP's Alto Tiete Hydrographic Region……...……..…32

Figure 6. The four selected ground stations in RJ's Baia de Guanabara Hydrographic Region…….…...32

Figure 7. NO_2 column grids in 2020 for SP (8a), RJ (8b); and 2015-2019 for SP (8c), RJ (6d)…….…….34

Figure 8. Yearly boxplots for daily ground data over selected SP stations……...……..36

Figure 9. Yearly boxplots for daily ground data over selected RJ stations…….37

Figure 10. Daily NO_2 concentrations during 2015-2020 at the Marginal Tiete Station in SP…….....…...38

Figure 11. Daily NO_2 concentrations during 2016-2020 at the DC Pilar Station in RJ…….38

Figure 12. Yearly boxplots for $PM_{2.5}$ daily ground data over selected SP stations.……...……...…….39

Figure 13. Yearly mean time-series for $PM_{2.5}$ daily ground data over single SP transport station……...……...40

Figure 14. Yearly time-series of mean NO_2 TVCDs over selected SP ground stations…….…....41

Figure 15. Yearly time-series of mean NO_2 TVCDs over selected RJ ground stations…….....42

Figure 16. Daily wind speeds averaged for the May month of 2015-2020 in SP……...43

Figure 17. Yearly mean air temperature for the month of May at selected RJ station ……..... 44

Figure 18. Number of fire hotspots in Southeast Brazil for the May months of 2015-2020……..44

Figure 19. Yearly mean air temperature for the month of May at selected RJ station..…….....45

Figure 20. Number of fire hotspots in Southeast Brazil for the May months of 2015-2020**…**……..46

Figure 21. Monitoring Air Stations and Fire Hotspots within SP state in 2019…….…….…...47

List of Tables

Table 1. Description of selected ground stations in SP ……..……. 30

Table 2. Description of selected ground stations in RJ ……..……..……....31

Table 3. NO_2 Correlation Data for the SP region ….....……..….. 41

Table 4. NO_2 Correlation Data for the RJ region …….42

Chapter 1 – Introduction

1.1 Overview

The purpose of this work is to explore the potential of satellite retrievals in monitoring atmospheric pollutant emissions while evaluating the effects of COVID-19 lockdown decrees in two main criteria air pollutants: Nitrogen Dioxide (NO_2) and particles less than 2.5 micrometers in diameter ($PM_{2.5}$). This was achieved by synergistically analyzing NO_2 satellite retrievals as well as ground-based measurements, correlating their year-to-year trends, and comparing them during different timeframes. For $PM_{2.5}$ we only analyzed surface data. The region of interest was the Brazilian states of Sao Paulo and Rio de Janeiro. This research document was organized in three main sections. Chapter 1 gives a background in available satellites, instruments, and data products that can be used for statistical analyses; Chapter 2 is the main body of this study including introductory information, materials and methods, results and discussion, and main findings from the research. Chapter 3 closes this thesis work with general conclusions and recommendations for future studies. By bringing up a specific case study using satellite data retrievals and ground measurements in an air quality context, this research aims to highlight the importance of filling the gaps in surface atmospheric databases by taking advantage of satellite instrumentation.

1.2 Background

1.2.1 Satellites

1.2.1.1 Definition

Man-made satellites can be defined as machines launched into space and orbiting around the Earth according to an article from the NASA Knows! Series (Stillman, 2014). They are carriers of important instruments within the air quality realm that serve a variety of purposes, including measuring vertical column densities of atmospheric trace gases.

Satellite machines acquire and send information back and forth to Earth and to be able do so, they mostly take advantage of an antenna and a power source. The former part is responsible to capture and transmit information, while the latter gives the machine the power needed to perform those functions. The power can be acquired from a solar panel or battery. For instance, NASA's AURA satellite has built-in solar panels.

1.2.1.2 Capabilities and characteristics

While retrieving data, satellite systems have a broad range of advantages that include, but are not limited to providing systematic data collection on established, repetitive, schedules; archiving data, which allows for the detection of previous pattern changes; worldwide coverage, depending upon specifics; having a broad customer base; and imaging remote regions on a regular basis (Stillman, 2014). On the other hand, they can also present difficulties, such as: substantial costs for satellite and instrumentation development, manufacturing, and operation; time-consuming system development and failures requiring expensive and more time-sensitive recovery.

These systems can be differentiated based on specific characteristics, such as: the orbit in which they are encountered; temporal resolution (i.e. revisiting times); altitude; inclination; spatial coverage; and customer base.

1.2.1.3 Satellite systems orbits

Satellite systems are projected to be launched and arrive at a specific orbit, also known as a trajectory around planet Earth. According to where these orbits reside, systems can be classified as: polar, non-polar/low Earth, geostationary, and sun-synchronous.

Polar-orbiting satellites are known to operate over the entire globe, including remote regions that would otherwise be difficult to reach at a surface-level. This is true because of their orbital plane placement, which is inclined at nearly 90 degrees to the equatorial plane. When moving within the orbit, satellites can go towards the north or south having the equator line as reference. An example of a polar-orbiting satellite system is the Suomi NPP.

Contrasting with polar orbits, satellite systems can take on non-polar orbit movement, also called a low-Earth orbit (LEO; usually less than 2,000km above the surface of the Earth). Data obtained from this setting is only available from a limited set of latitude locations. An example here is the Global Precipitation Mission (GPM).

Aside from polar/non-polar, geostationary or geosynchronous satellites do not gather data at different locations during its rotation, but instead captures the same Earth view with each retrieval as they follow the Earth's rotation. This translates in continuous coverage of one area. For instance, the Geostationary Operational Environmental Satellite (GOES) captures weather information for a specific location.

Sun-synchronous orbits also follow Earth's rotation, but with respect to its solar beam angle. In other words, these satellite systems rotate at the mean rate of the Earth about the Sun. They are designed such that each orbital satellite pass on the daylight side of the Earth is shifted westward to minimize variation in sun angle at local sun time. Most of the polar-orbiting satellites are also classified as sun-synchronous, which results in data retrievals all over the globe but at one

continuous specific location and at the same solar time for each crossing. An example of a sun-synchronous and polar satellite system is the Landsat series system, used effectively to track land use changes.

1.2.1.4 Satellite systems examples

Effectively monitoring the entire Earth is very expensive: no country alone can afford to do that. This is why different countries have their own efforts on satellite building and monitoring. International cooperation is a must. In the United States, NOAA operates Suomi NPP while AQUA and TERRA were launched by NASA but have instruments from the United States, Japan, and Canada. AURA is operated by NASA, and Sentinel-5 is part of the European Earth Observation Programme "Copernicus", which is a coordinated and managed by the European Commission (EC). CALIPSO is a joint mission between NASA and the French Space Agency.

Information about some of the satellite systems specifications can be found in Appendix A.

1.2.2 Satellite Systems Instruments

Satellite systems have scientific instruments, or sensors, built-in them. Those instruments can acquire data from space and send it to Earth through the satellite antennas. There are two types of remote sensing sensors: passive and active.

Instruments that do not have a built-in source of illumination to detect radiation from objects/scenes of interest are called passive. Instead, they take advantage of natural reflected sunlight to operate. Conversely, active sensors provide their own light source, sending a pulse of energy from the sensor in the direction of the observed object, and receiving radiation reflected or backscattered from the objects being observed.

Each instrument/sensor works in a different wavelength range of the electromagnetic spectrum. For this reason, it is useful and clarifying to define what is an electromagnetic spectrum before explaining more about which regions the sensors work at.

1.2.2.1 Electromagnetic energy

Electromagnetic energy is produced by the vibration of charged particles. It travels in the form of waves throughout the atmosphere and space vacuum. Oscillation charges produce steady sources of electromagnetic waves. When these are radiated, the electric charges lose energy. Difference in wavelengths (frequencies) is caused by differences in the rate of oscillations: fast oscillations, caused by small electric charges, produce small wavelengths (high frequencies), while slow oscillations, caused by large electric charges, produce longer wavelengths (low frequencies).

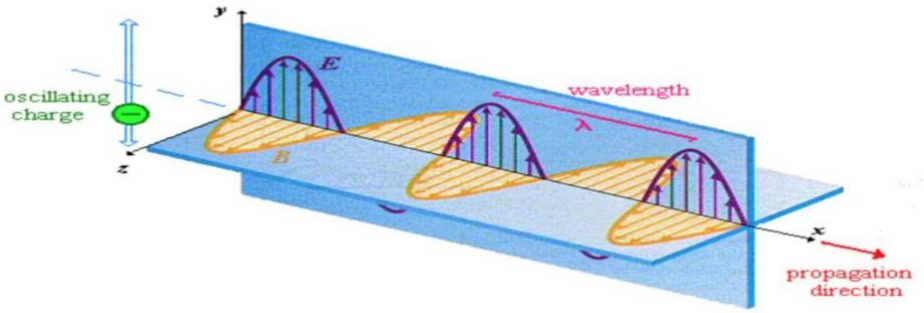

Figure 1. *Electromagnetic wave. (*Source: Campbell, J. and Wynne, R., *Introduction to Remote Sensing Textbook*, 2011, Guilford Press., New York. ISBN: 1-57230-040-8).

Electromagnetic radiation can have different intensities over time or distance. They are characterized by the following properties:

I. Wavelength (λ): distance from crest to crest
II. Frequency (v): number of crests passing a fixed point over a given period of time
III. Amplitude (A): height of each peak
IV. Speed (s): constant at 299,893 km/s

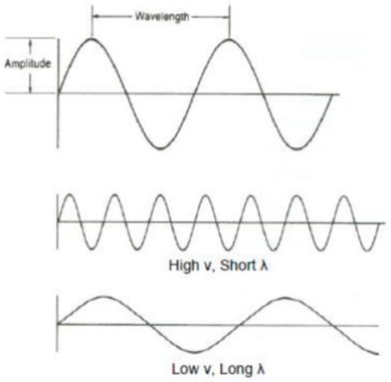

Figure 2. *Wave characteristics.*(Source: Campbell, J. and Wynne, R., *Introduction to Remote Sensing Textbook*, 2011, Guilford Press., New York. ISBN: 1-57230-040-8).

The following figure helps on the identification of different wavelengths and their respective frequencies. Visible light is situated mid-range in the electromagnetic spectrum. Satellite instruments usually perform near the microwave and infrared parts of the light spread.

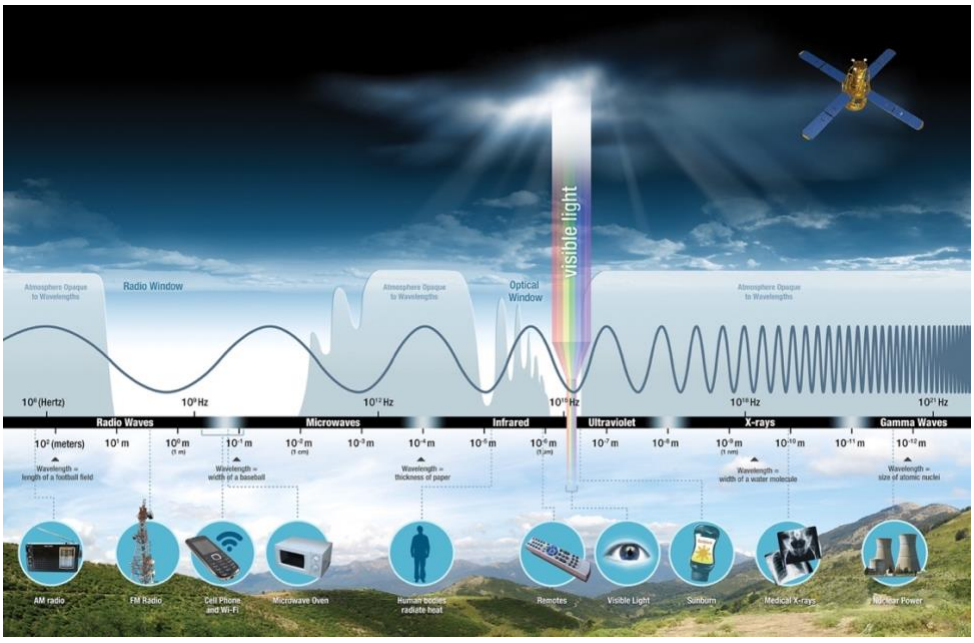

Figure 3. *Electromagnetic Spectrum* (Source: Berrick, Stephen. "What is Remote Sensing?", *NASA's Earth Data: Open Access for Open Science*, 2020, http://earthdata.nasa.gov/learn/backgrounders/remote-sensing/).

When electromagnetic radiation reaches a target, it can have three different general types of interaction with it:

I. Absorption: retention of radiated energy.

II. Reflection: radiated energy hits the object and bounces off.

III. Transmission: passage of radiated energy through the object.

Each target has a characteristic interaction with radiation wavelengths, which makes possible the definition of a "spectral fingerprint" for each object of interest in Earth, including air pollutants. The most common types of radiation-air pollutant interactions are absorption and scattering. The two major categories are defined for scattering: Rayleigh and Mie. The former occurs from molecules (e.g. NO_2) and very tiny particles (diameter < 1/10 of wavelength light), while the latter is sourced in larger particles, like $PM_{2.5}$. Both are classified as elastic forms of scatter with incident wavelengths unchanged.

1.2.2.2 Instrument categorization

Sensors may be categorized based on the wavelength range at which they operate. As an example, active sensors tend to operate in the microwave portion of the electromagnetic spectrum, and thus are able to use their light to penetrate into the atmosphere under harsh conditions, capturing back the reflected/refracted/scattered radiation. Passive instrumentation, however, typically operate in a wider range of the spectrum, including visible, infrared, thermal infrared, and microwave. All of these options provide the sensor with its lighting needs for optimal performance. Light Detection and Ranging (LiDARs) and scatterometers are categorized as active instruments, while imaging spectroradiometers, spectrometers, radiometers, and atmospheric sounders are passive.

For air quality measurements of $PM_{2.5}$, and NO_x, the most used instruments are: imaging spectroradiometer (with MODIS and MIRS for AOD), imaging spectrometer (with OMI for AOD

and NO_x; TROPOMI, OMPS and SAGE III for NO_x), imaging radiometer (with VIIRS and CALIPSO for AOD), and LiDAR (with CALIOP for AOD).

Some instrumentation may have different types of sensors attached in one system. For example, the CALIPSO platform includes an imaging radiometer, a LiDAR, and a wide-field camera. In this case, all of the modules operate autonomously and continuously, although the camera acquires data only under daylight conditions.

For further information on how each instrument works and example specifications, Appendix B can be consulted on this document.

1.2.3 Instrument Data Products

1.2.3.1 Product Level Classification

All instruments onboard of satellites collect data that is sent to Earth and used by researchers, decision makers, and society at large. However, before they can be used, raw data need to be processed to be converted into more useful parameters and formats.

Depending on the degree at which the data is processed, it can be classified in different levels:

I. Level 0 (L0): raw data at full instrument resolution,

II. Level 1A (L1A): unprocessed data at full instrument resolution, but now time-referenced and annotated with ancillary information such as radiometric and geometric calibration coefficients and georeferencing parameters,

III. Level 1B (L1B): level 1A data that have been processed to sensor units (e.g. radar backscatter cross section, brightness temperature, etc.),

IV. Level 2 (L2): derived geophysical variables at the same resolution and location as Level 1 source data,

V. Level 3 (L3): variables mapped on uniform space-time grid scales, usually with some completeness and consistency,

VI. Level 4 (L4): model output or results from analyses of lower-level data (e.g., variables derived from multiple measurements).

1.2.3.2 Relevant Data Variables

For the NO_x measurements, NO_2 is the element usually measured since NO is converted to NO_2 in the presence of sunlight (and vice-verse) on a timescale of minutes.

NO_2 is measured by the following instruments:

I. OMI

II. TROPOMI

III. OMPS

IV. SAGE III

Each satellite instrumentation takes advantage of different algorithm developments for retrievals. The algorithm method used by OMI for NO_2 retrievals will be further explained in the following section.

1.2.4 $OMNO_2$ retrieval algorithm

The $OMNO_2$, the standard operational OMI NO_2 data product algorithm used for NO_2 slant column retrievals, has had a few versions made available throughout the last couple of years (Krotkov et al., 2020; Krotkov et al., 2019; Bucsela et al., 2013). Each bring some procedure modifications compared to the previously released version. With the goal of introducing precursory algorithm methodology information and then further explaining the next release being used in the present study, Version 2.1 of the OMI product (or SP2) will be summarized first.

1.2.4.1 SP2 Summary

The SP2 takes advantage of the stratosphere-troposphere separation (STS) algorithm to distinguish the total slant column (initially approximated as stratosphere) from the respective tropospheric pollution. However, before any separation procedure is performed, the resulting strips generated by calibration biases of cross-tracked field of views in the instrumentation are removed by calculated correction constants applied to each pixel in the orbit. NO_2 columns are retrieved based on air mass factors (AMF), or the ratios between slant and vertical columns, that are a function of previously modeled NO_2 mixing profiles, radiate transfer calculations, and terrain reflectivity. The mathematical steps involved in the STS depend on previously modeled tropospheric NO_2 (modtopNO2). Where there is little of that component, the initial vertical column is subtracted from modtopNO2 and the stratospheric vertical column can be obtained. Further spatial smoothing and interpolation procedures are taken after that. On the other hand, if there is a lot of modtopNO2, first the stratospheric fraction is computed with spatial interpolation and then the tropospheric NO_2 column can be obtained by subtracting the initial vertical column from the calculated stratospheric fraction (Bucsela et al., 2013).

It is important to note that the initial NO_2 slant column (obtained before the AMFs) are estimated based on the DOAS method, that uses a normalized spectra based on previously fitted laboratory-measured trace gas absorption spectra. The resulting spectral fit is the raw slant-column density for each OMI pixel. Another interesting remark is the determination of an absolute threshold until where stratospheric NO_2 absorption can be taken by tropospheric values. This limit allows for the initial estimate of the vertical columns.

1.2.4.2 Sources of Error

Uncertainties associated with the NO_2 slant column retrievals can be related to different parts of the algorithm procedure: the spectral fitting, the STS algorithm, and the AMFs.

Since multiple slant columns are retrieved for the algorithm, the associated spatial information, climatology and the *a priori* NO_2 vertical mixing profile are prone to assumption errors. Those lead to misleading of the AMFs, that are calculated based on the mixing profiles generated from chemical transport models (CTM). Other error sources encountered in AMFs come from scattering weights, temperature profile, terrain albedo, tropopause pressure, and cloud pressure/fraction. In terms of magnitude, it was generally assumed by Wenig et al. (2008) hat AMFs tropospheric uncertainties can be up to 20% in a clear-sky, assuming a terrain reflectivity of ~0.015.

In addition to AMFs, geographic/weather data and tropospheric modeling can affect the stratospheric column estimate during the STS separation procedure. When the masking step is performed, *a priori* tropospheric contamination is taken into account and analyzed if it exceeds a certain threshold to be masked and further interpolated. Errors in the thresholds retrievals can affect that and further in the process when any hot spots areas are eliminated within the stratospheric field. Geographic averaging functions and random inaccuracies from differences between monthly mean climatology and daily tropospheric profiles in CTM may also be affected. A general estimation for the magnitude of errors in the stratospheric column estimate is about 0.2 x 10^{15} cm^{-2}. This value is usually associated with the masking threshold adopted for the vertical columns. By taking in account all uncertainties described for the NO_2 vertical columns, a general magnitude error value of 1 x 10^{15} cm^{-2} is taken by Bucsela et al. (2013) for clear skies.

1.2.4.3 Satellite Retrieval Differences from Aircraft, Ground and Modeled NO_2 retrievals

Aircraft, ground, and modeled NO_2 datasets serve as good validating measurements for OMI tropospheric NO_2. On the other hand, satellite retrievals can be a reference for model results evaluation and further help on the algorithm used to obtain OMI NO_2 data itself.

Lamsal et al. (2014) compared NO_2 satellite retrievals to aircraft, ground-based, in situ surface measurements and a bottom-up emission inventory. The ground data, measured by MAX-DOAS (measures scattered sunlight over UV/visible wavelengths) and Pandora (spectrometer measuring solar irradiance) was used to assess data quality. Aircraft data was used to compare satellite columns and assess sensitivity of the retrievals to previously modeled NO_2 vertical profiles. High-resolution NO_2 profile models were also used to investigate improvements on the standard retrieval algorithm. These models were also adopted to estimate tropospheric columns from in situ ground measurements. Results showed aircraft agreed on modeled NO_2 vertical profiles in about 30%, while this percentage compared to OMI retrievals is of about 20%, with lower biases close to rural locations. Now ground-based Pandora and OMI data comparison seemed to be inconsistent in the short-term period of time, in addition to ground-pixel lack of spatial representativity and STS errors, and differences in sample domains. Therefore, it is important to note that adopting a broad timeframe, with significant spatial correspondence between ground and satellite and sample homogeneity are adamant to a robust ground-satellite comparison of NO_2 measurements. Another relevant statement is that the MAX-DOAS ground measurements showed higher correlation to the OMI satellite data than Pandora.

When surface NO_2 derived from OMI was compared to surface measurements in the same study, the biggest difference was found during winter at a specific location (~31%). Also, when bottom-

up local NO_2 ground measurements were added to surface data, a range of 44% was found for two different seasons, and the biggest difference found was during Spring.

Bucsela et al. (2013) also highlighted comparisons of OMI measurements amongst different NO_2 retrieval algorithms. Their results showed similar qualitatively synoptic structures between the model and SP2, while SP1 (or the Version 1.0 of the $OMNO_2$ data algorithm) did not show good agreement with the stratospheric NO_2 modeled and retrieved from the SP2 algorithm. A wave-2 assumption has been highlighted as a potential source of error in SP1. It is related to a zonal variation using simplistic assumptions within stratospheric field. The OMI Dutch DOMINO algorithm, also used for NO_2 retrievals, showed the same wave error and stronger diurnal variation compared to SP2. Even though these differences were noted, the tropospheric slant column of all algorithms are qualitative similar to the modeled one. Still, SP2 showed less negative values associated with the NO_2 slant columns. Still according to Bucsela et. al (2013), these negative measurements can be associated with cloud, snow, result of row anomaly or binding/interpolating/smoothing product generating a vertical stratospheric column bigger than the adopted initial total vertical column.

1.2.4.4 Version 3.0 $OMNO_2$ data product improvements

From SP2, the $OMNO_2$ algorithm version 3.0 (SP3) brings the following major improvements, as stated in Kroktov et al. (2017):

1) New spectral fitting approach that corrects some issues from the DOAS technique. This allowed less sensitivity to the spectral fitting window with a multi-step, iterative retrieval for all species within the wavelength range.

2) A priori modeled NO_2 and temperature profiles with higher spatial resolution. This helps on more accurate calculation of AMFs, and thus more accurate stratospheric/tropospheric separation.

Overall, the SP3 showed a significant reduction in vertical columns, with tropospheric retrievals being most affected by the algorithm changes. Kroktov et al. (2017) highlighted ~ 2-5 x 10^{15} cm^{-2} reductions over Europe with the adopted modifications. Although the changes are big, the confidence in attributing values to NO_2 vertical columns around the globe is higher with the algorithm improvements reducing uncertainties related to DOAS and modeled vertical profiles.

1.2.5 Review of the Application of Satellite Data in Monitoring Air Pollution

Satellite data has been increasingly used worldwide to provide measurements of air pollutant levels in the past two decades (Duncan et al., 2014). Specifically, satellite retrievals have been considered as complimentary tools to traditionally used ground-based observations in recent years. For example, a study in China (She et al., 2020) used AOD satellite data to increase temporal and spatial coverage within regions lacking ground monitoring stations. In Brazil, a study (Oliveira et al., 2019) analyzing AOD properties from different instruments was done aiming to serve as the initial step to further validate models of $PM_{2.5}$ concentrations. Ground-based measurements from monitoring stations, like from Purple Air sensor stations, have been combined with satellite data and model outputs. This procedure gives less uncertainty associated with the resulted pollutant concentrations. For instance, a recent study of $PM_{2.5}$ concentrations in New York City (Huang et al., 2019) added non-regulatory measurements to a satellite-based model and found different spatial patterns and supplemental pollution hotspots where the non-regulatory measurements were retrieved from, in particular for densely populated areas and major roads. Besides that, higher

standard deviations and 95th percentiles between the AOD and non-AOD daily model were found in areas with fewer $PM_{2.5}$ monitors.

OMI data was also used in two recent NO_x studies, one in Kazakhstan (Darynova et al., 2018) and one in Switzerland (Hoogh et al., 2019). The former obtained tropospheric NO_2 to identify major NO_2 hot spots, trends, and seasonal variations over the country. Currently, the number of monitoring stations in Kazakhstan is not sufficient, even though the pollutant concentrations often go above the healthy levels. From their analysis, a wintertime peak of NO_2 was found for hotspot cities due to the increased need of heat and increased lifetime of NO_2. They suggest that their work could be followed by studies adding ground-based monitoring data, model estimates of column NO_2, and/or other satellite products such as TROPOMI. Furthermore, the transboundary influence of other countries in NO_2 levels was also proposed for future studies. Hoogh et al. (2019) not only obtained NO_2 satellite measurements, but also applied a multistage modeling framework to downscale the retrievals and combine them with ground data. Their results showed 58% of correlation between the satellite model results and actual data, and 73% for the resultant residual variation between ground source data and the combined data.

1.3 Objectives

The main goal of this thesis research is to explore the potential of satellite retrievals when used together with ground measurements to evaluate NO_2 and $PM_{2.5}$ concentrations before and during COVID-19 lockdown in the Sao Paulo (SP) and Rio de Janeiro (RJ) states of Brazil. To achieve this goal, the following steps are taken as described, in details, in the following chapter:

I. Gather OMI satellite NO_2 data product (OMINO2d), and NO_2 and $PM_{2.5}$ ground measurements from NASA and Brazilian environmental agencies, respectively.

II. Average, re-grid, and analyze daily satellite data.

III. Analyze daily ground data for different timeframes and stations.

IV. Investigate the correlation between year-to-year trends of satellite NO_2 column grid and ground measurements.

V. Analyze meteorological data and investigate the potential role of weather conditions in changes of pollutant levels.

References

Berrick, Stephen. “EOSDIS Distributed Active Archive Centers (DAACs)”. NASA’s Earth Data: Open Access for Open Science. Last updated on July 29, 2020. Accessed December 02, 2020. https://earthdata.nasa.gov/eosdis/daacs/.

Berrick, Stephen. “Health and Air Quality Data Pathfinders”. NASA’s Earth Data: Open Access for Open Science. Last updated on Oct 16, 2020. Accessed December 02, 2020. https://earthdata.nasa.gov/learn/pathfinders/health-and-air-quality-data-pathfinder/.

Berrick, Stephen. "What is Remote Sensing?”. NASA’s Earth Data: Open Access for Open Science. Last updated on Nov 17, 2020. Accessed December 02, 2020. https://earthdata.nasa.gov/learn/backgrounders/remote-sensing/.

Berrick, Stephen. “Data Tools”. NASA’s Earth Data: Open Access for Open Science. Last updated on Oct 29, 2020. Accessed December 02, 2020. https://earthdata.nasa.gov/earth-observation-data/tools/.

Bucsela, E. et al. “A new stratospheric and tropospheric NO2 retrieval algorithm for nadir-viewing satellite instruments: applications to OMI”. *Atmospheric Measurement Techniques.* 6 (2013): p. 2607-2626 . doi:10.5194/amt-6-2607-2013.

California Institute of Technology: Jet Propulsion Laboratory. “MISR Instrument”. NASA. Accessed December 02, 2020. https://misr.jpl.nasa.gov/Mission/misrInstrument/.

California Institute of Technology: Jet Propulsion Laboratory. “The EOS MLS Instrument”. NASA. Accessed December 02, 2020. https://mls.jpl.nasa.gov/eos/instrument.php/.

Campbell, J. , and Wynne, R. 2011. *Introduction to Remote Sensing*. New York: Guilford Press. 666 p. (5th ed.) (ISBN: 1-57230-040-8).

Darynova, Z. et al. “Evaluation of NO2 column variations over the atmosphere of Kazakhstan using satellite data”. *Journal of Applied Remote Sensing* 12 (2018): n. 4, p. 042610.

De Hoogh, K. et al. “Predicting Fine-Scale Daily NO2 for 2005-2016 Incorporating OMI Satellite Data Across Switzerland”. *Environmental Science & Technology* 53 (2019): n. 17, p. 10279-10287.

De Oliveira, A. et al. “Analysis of Atmospheric Aerosol Optical Properties in the Northeast Brazilian Atmosphere with Remote Sensing Data from MODIS and CALIOP/CALIPSO Satellites, AERONET Photometers and a Ground-Based Lidar”. *Atmosphere* 10 (2019): p. 594.

Duncan, B. et al. “Satellite data of atmospheric pollution for U.S. air quality applications: Examples of applications, summary of data end-user resources, answers to FAQs, and common mistakes to avoid”. *Atmospheric Environment* 94 (2014): 647-662. doi.org/10.1016/j.atmosenv.2014.05.061.

Duncan, Bryan. “Ozone Monitoring Instrument (OMI)”. NASA’s Aura webpage. Accessed December 02, 2020. https://aura.gsfc.nasa.gov/omi.html.

Duncan, Bryan. “Tropospheric Emission Spectrometer (TES)”. NASA’s Aura webpage. Accessed December 02, 2020. https://aura.gsfc.nasa.gov/tes.html/.

Frazier, Shannell. “Specifications”. NASA’s MODIS Web. Accessed December 02, 2020. https://modis.gsfc.nasa.gov/about/specifications.php/.

Huang, K. et al. “Estimating daily PM 2.5 concentrations in New York City at the neighborhood scale: Implications for integrating non-regulatory measurements”. *Science of the Total Environment* 697 (2019): p. 134094.

Koninklijk Nederlands Meteorologisch Instituut: Ministerie van Infrastructuur en Waterstaat. “KNMI - TROPOMI”. Accessed December 02, 2020. https://www.knmi.nl/kennis-en-datacentrum/uitleg/tropomi/.

Krotkov, N. et al. The version 3 OMI NO2 standard product. *Atmospheric Measurement Techniques Discussions,* in review, 2017. doi:10.5194/amt-2017-44.

Krotkov, N. et al. OMI/Aura NO2 Cloud-Screened Total and Tropospheric Column L3 Global Gridded 0.25 degree x 0.25 degree V3. NASA Goddard Space Flight Center: Goddard Earth Sciences Data and Information Services Center (GES DISC), 2019. Accessed March 3rd, 2020. 10.5067/Aura/OMI/DATA3007/.

Lamsal, L. N. et al. OMI/Aura Nitrogen Dioxide Standard Product with Improved Surface and Cloud Treatments, *Atmospheric Measurement Techniques Discussions*, doi: 10.5194/amt-2020-200, 2020.

McPeters, Rich. “OMPS Nadir Mapper Level 2 Description”. NASA’s Ozone & Air Quality Media Docs. Accessed December 02, 2020. https://ozoneaq.gsfc.nasa.gov/media/docs/NMTO3-L2_Product_Description.pdf/.

Santosh, R., “Satellite Remote Sensing” (class lecture, Advanced Remote Sensing, Virginia Polytechnic Institute and State University, Blacksburg, Virginia, Spring 2020).

She, Q. et al. “Satellite-based estimation of hourly PM 2.5 levels during heavy winter pollution episodes in the Yangtze River Delta, China”. *Chemosphere* 239 (2020): p. 124678.

Stillman, Dan. "What is a Satellite?" NASA Knows! (Grades 5-8). NASA, Feb.12, 2014. https://www.nasa.gov/audience/forstudents/5-8/features/nasa-knows/what-is-a-satellite-58.html/.

Trepte, Charles. “Cloud-Aerosol Lidar and Infrared Pathfinder Satellite Observations”. *NASA*, December 11, 2020. https://www-calipso.larc.nasa.gov/about/.

U.S. Environmental Protection Agency. "Criteria Air Pollutants”. Accessed December 2, 2020. https://www.epa.gov/criteria-air-pollutants/.

Wenig, M. O. et al. “Validation of OMI tropospheric NO2 column densities using direct-sun mode Brewer measurements at NASA Goddard Space Flight Center”. *Journal of Geophysical Research* 113 (2008): D16S45. doi:10.1029/2007JD008988, 2008.

Wolfe, Robert. “Visible Infrared Imaging Radiometer Suite (VIIRS)”. NASA’s Distributed Active Archive Center. Accessed December 02, 2020. https://ladsweb.modaps.eosdis.nasa.gov/missions-and-measurements/viirs/.

World Meteorological Organization. “Welcome to OSCAR”. OSCAR webpage: Observing Systems Capability Analysis and Review Tool. Accessed December 02, 2020. https://www.wmo-sat.info/oscar/.

Chapter 2. Atmospheric Pollutant Levels in Southeast Brazil During COVID-19 Lockdown: Combined Satellite and Ground-based Data Analysis

Rayssa Brandao and Hosein Foroutan

Department of Civil and Environmental Engineering, Virginia Tech, Blacksburg, Virginia 24061, USA

This chapter of the thesis is in preparation to be submitted as a manuscript to the *Science of the Total Environment*.

2.1 Abstract

With the ongoing COVID-19 pandemic being spread all over the world, lockdown measures are being implemented making air pollution levels go down in several countries. In this context, the air quality changes in the highly populated and trafficked Brazilian states of São Paulo (SP) and Rio de Janeiro (RJ) were addressed using a combination of satellite and ground-based daily data analysis. We explored nitrogen dioxide (NO_2) and particulate matter ($PM_{2.5}$) daily levels for the month of May during different years within 2015-2020. Daily measurements of NO_2 column concentrations from the Ozone Monitoring Instrument (OMI) aboard NASA's Aura satellite were also gathered and averaged decreases of 42% and 49.6% were found for the year of 2020 compared to previous averaged 2015-2019 years. In parallel to the NO_2 column retrieval, the ground-based data, measured by the Brazilian States Environmental Institutions, was analyzed, and correlated with satellite retrievals. Correlation coefficients between year-to-year changes in satellite column and ground-based concentrations were 77% and 53% in SP and RJ, respectively. It was found a 13.3% (p-value = 0.099) and 18.8% (p-value = 0.077) decrease in NO_2 levels for SP and RJ, respectively, in 2020 compared to 2019. For $PM_{2.5}$, no significant change was observed in 2020 compared to 2019 for the SP region. To further isolate the effect of emissions reduction due to the lockdown, the meteorological fields and number of wildfire hotspots were analyzed. No interference of weather or wildfire emissions was found on NO_2 ground levels in 2020 compared to previous years, while the $PM_{2.5}$ concentration distributions suggested an influence by the wildfires in the Southeast region of the country. The integrated analysis of satellite and ground-based measurements is innovative and has to be further explored in Brazilian studies. This is true especially because the ground-based stations are spatially and temporally sparse in Brazil.

2.2 Introduction

The new coronavirus (COVID-19) disease was declared as a global pandemic by the World Health Organization (WHO) on March 11, 2020 (WHO, 2020). Since then, several countries that had not yet adopted social isolation measures have been promulgating lockdown decrees to avoid the spread of the virus. In Brazil, small towns to bigger cities and entire states have implemented lockdown regulations in varying time frames and social-economic activities, depending on local virus propagation, infrastructure and regional characteristics (Croda et al., 2020).

The Southeastern states of São Paulo and Rio de Janeiro were the first ones to implement lockdown measures on local areas due to their high numbers of COVID-19 cases. Considering that they are highly populated, industrialized regions and hold the largest economic clusters in the nation, any imposed changes on their regular activities would greatly affect the country's GDP (gross domestic product). Therefore, no lockdown sanction was determined for industries (Siciliano et al., 2020b). On the other hand, public transport was limited and private vehicles had to go through a system of traveling only when their registration plate matched certain digits defined by the State Administration for specific weekdays.

Automobiles are known to emit several air pollutants including carbon monoxide (CO), carbon dioxide (CO_2), volatile organic compounds (VOCs) or hydrocarbons (HCs), nitrogen oxides ($NO + NO_2$), and particulate matter (PM) (Transportation Research Board, 2002). When vehicle activity is limited by measures such as the COVID-19 lockdown, it is only logical to assume that traffic-related air pollutant levels will go down. A recent study by Nakada and Urban (2020) highlighted the air quality impacts of a partial lockdown in the São Paulo State. They found >50% lower concentrations of traffic-related pollutants (CO, NO_x) during quarantine (March 24 – April 20, 2020) compared to a five-year mean for the same days of the month based on four ground-

based stations. All chosen stations were located in roads or close to where high traffic levels are located (highly urban stations). Another study applied to Brazil (Dantas et al., 2020) shows decreases in the Rio de Janeiro State for CO and NO_2 during lockdown. However, these pollutants presented lower percentage reduction in 2020 if compared to the São Paulo study. Another difference between the latter studies is that the comparison of 2020 mean pollutant levels was only to 2019 averages for Rio data, while for Sao Paulo the previous 2015-2019 data years were taken into consideration. Ozone (O_3) levels raised up in both studies, and that was associated with the decrease in NO_x. In the Rio study, the additional effect of a VOC-controlled atmospheric environment in the O_3 formation was also mentioned. Furthermore, the ground-based Rio stations were also all located close to vehicular flux (moderate to high in urban areas).

Besides Brazil, other countries have been highlighting air pollutant level decreases in urbanized areas during COVID-19. Tobías et al. (2020) described significant lower NO_2 and BC concentrations during lockdown compared to a couple weeks before in busy locations in Barcelona, Spain. Kumar (2020) found lower NO_2 and AOD concentrations from satellite retrievals for six megacities in India when the lockdown period was compared to the same weeks from the previous three years. Yuan et al. (2020) and Ghahremanloo et al. (2020) call attention for particularly high decreases in NO_x for East Asia regions when pre-COVID months are compared to local lockdown timeframes. In the U.S., two studies (Liu et al., 2020; Berman and Ebisu, 2020) comparing 2020 lockdown months to the same weeks in previous years showed decreases in NO_2 and $PM_{2.5}$.

Trends in NO_x gases emissions have been receiving more attention than usual due to its applicability to area sources (i.e. many, small, and widespread) and the potential use of satellite data for estimating those emissions (Duncan et al., 2014). NO_2, defined by EPA as a primary

criteria pollutant, is broadly released to air from the burning of fuel, and thus greatly related to traffic pollution worldwide. Its short chemical life-time, according to Duncan et al. (2014), allows surface emission data to be well correlated with tropospheric NO_2 vertical column densities (VCDs), which are concentrations measured by satellite and converted from a slant plane to a perpendicular position in relation to the Earth's surface. While this correlation is demonstrated, NO_2 VCDs become an important proxy of surface data, especially when ground-based stations are sparse and/or inactive over an area of interest. This way when ground-based data is missing, NO_2 VCDs might be able to fill the gaps and provide a NO_x estimate for crucial polluted locations. Although several studies have shown the temporal correlation potential between NO_2 ground and satellite column concentrations (Bechle et al., 2013; Rivera et al., 2013; Petritoli et al., 2004; Oner and Kaynak, 2016), no studies applied to Brazil have this statistical analysis yet.

In addition to NO_x, airborne particulate matter is widely associated with road traffic emissions, particularly from diesel vehicles. $PM_{2.5}$ particles in specific are of concern because of their health effects when penetrated deeply into the human lungs. These particles are not only directly emitted from tailpipes of cars, but also resuspended from roads and can be formed by NO_x and VOC gases (US EPA, 2020). According to a study review done for the U.S. by Hodan and Barnard (2004), the "formation of $PM_{2.5}$ from NO_x and VOC chemicals vary greatly in the country, from approximately 4% to 37%". Although it is hard to identify the exact $PM_{2.5}$ amount initiated by NO_x, Hodan and Barnard estimated that $PM_{2.5}$ emissions from traffic account for 20% of total $PM_{2.5}$ emissions. For Brazil, Andrade et al. (2012) found vehicle emissions contribute to at least 40% of the $PM_{2.5}$ mass in six metropolitan cities including Sao Paulo and Rio de Janeiro. Therefore, it is relevant to take PM particles into account when a traffic-related study is developed.

For research on air quality during COVID-19 lockdown, $PM_{2.5}$ estimates become relevant since restrictions on transportation are being constantly made in various levels and at different locations. Although a lot of recent research has been addressing COVID-19 lockdown effects on regional air quality, several papers show limited results by not quantifying meteorological effects that might, and most likely will, influence pollutant concentration variation for a fixed period of time. Some are doing it using a modelling approach. Shen et al. (2020) inputted observational data in a FLEXPART-WRF model and demonstrated the impacts of regional transport on local air quality. They stated the importance of meteorology in air pollution events during the lockdown in Central China. Another study from China (Zhao et al., 2020) found substantial changes in NO_2 and O_3 when meteorological effects were isolated and taken out of their CMAQ modelling. It is important to note, however, that modeling practices bring uncertainties with them. For instance, as Zhao et al., (2020) mentioned: "WRF and other regional models have difficulties in simulating the evolution of the boundary layer". Modeling input variables themselves bring uncertainties to the model. Sensitivity analysis is a must for the evaluation of simulation models.

Another limitation some papers present is on short timeframes chosen for contrasting air pollutant levels. By using only 2020 months, the variation within different years is not captured, which is a key in detecting year-to-year differences, as well as the impact of any interference of local events/ or government decrees on the air quality during COVID. Furthermore, having a broader set of meteorology data helps in understanding the behavior of pollutants up to the current year, and if there are any correlations between those patterns. In this paper we compare monthly average of NO_2 and $PM_{2.5}$ concentrations during the average of five months of May (2015-2019) to the May 2020. This timespan was selected after reviewing local lockdown decrees timeframes and comparing daily NO_2 columns plots averaged for different lockdown weeks.

The areas of interest adopted for the present study are the Brazilian states of Sao Paulo and Rio de Janeiro, with their hydrographic regions delimited and metropolitan areas focused on when quantitative analyses were performed.

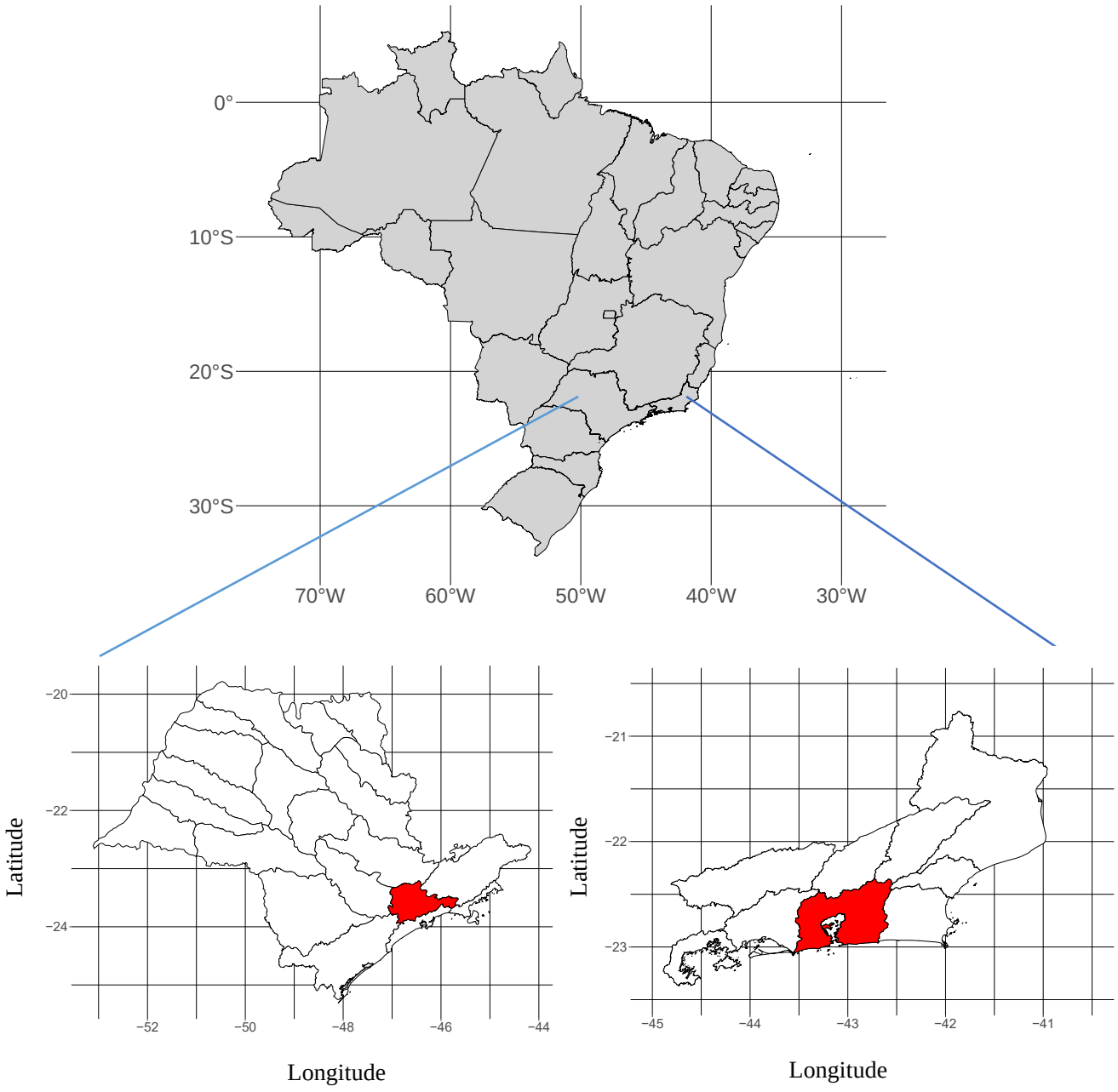

Figure 4 – Selected Brazil states (SP and RJ) and their hydrographic regions (chosen hydrographic units highlighted in red)

The main goal here is to address NO_2 and $PM_{2.5}$ concentration changes before and during COVID-19 lockdown using a combined analysis of both satellite and surface air data. This does not refer to direct overlaying of both data sources. Instead, combined data analysis here is referring to a common pattern or behavior found within the two data sources and their statistical comparison. By correlating numbers from different pollutant data sources we aim to bring up the importance of satellite retrievals at places where ground stations are non-existent. In addition, the effect of meteorological variables and natural fire emissions on the findings will be evaluated.

2.3 Material and Methods

2.3.1 Satellite Retrievals of Tropospheric NO_2

The OMI instrument, on board of NASA's EOS AURA satellite, is a nadir-viewing near-UV/Visible charge-coupled device spectrometer (264-504 nm spectrum) and was hereby adopted for NO_2 Column Density retrievals. OMI was launched on July 15, 2004 and is still operating providing daily measurements of key air quality components, including NO_2, throughout the whole globe. It orbits the Earth in accordance to AURA's polar Sun-synchronous pattern. Its field of view (FOV) is approximately 13 km x 24 km near nadir and its local equator crossing time (LECT) is 13:45 ± 0:15. For our study area in Brazil, the overpassing time was approximated to be thirty minutes after LECT, or 14:15 ± 0:15, in accordance with the OMNO2 user's guide (Krotkov et al., 2017) for Southern Hemisphere regions.

The OMNO2d variable of interest is a Level-3 grid and was acquired from NASA's GES DISC Version 3.0 Data Product release (Krotkov et al., 2020). There are different column retrieval options within OMNO2, but the selected one for this study was the NO_2 Tropospheric Column (TVCD). By choosing the tropospheric instead of total column, the stratospheric NO_2 column

amount is removed, bringing the pollutant measurements closer to emission sources. There was an additional selection option for grid files containing cloud-fractions less than thirty percent, but the tested results were the same as the grids containing clouds. Thus, cloud cover shouldn't be a problem for our datasets. The original TVCDs files were in the HDF-EOS version 5 format, but were exported as NetCDF files. The data grids had a spatial resolution of 0.25° x 0.25° latitude-longitude (= 13 km x 24 km), or the instrument's FOV, which is equivalent to the Earth's surface area covered by one pixel. That means for our region of interest ($\sim$7947 km^2 in Metropolitan Region of Sao Paulo – RMSP, and $\sim$7536 km^2 in Metropolitan Region of Rio de Janeiro - RMRJ), each pixel represents 13 km of our area on the y-direction and 24 km on the x-direction.

The five-year averaged NO_2 range for RJ presented negative values at some grid cells, but this was attributed to the retrieval algorithm, when the tropospheric column is calculated from the difference between a large value of stratospheric columns and the total column. The detailed algorithm can be found in Bucsela et. al (2013).

2.3.2 Satellite Data Analysis

To be able to have a big picture of the NO_2 TVCDs before and during the COVID-19 lockdown decrees, the OMNO2d daily files were averaged for the May months of 2015-2019 as well as for May 2020, using the NetCDF Ensemble Average Operator (ncea from the NCO package). After obtaining a single averaged file for the five-year period and 2020, the RStudio Software (V. 1.2.1) was used to plot the NetCDF files into a latitude-longitude grid.

In addition to spatial plots, NO_2 mean column values were obtained for grid cells surrounding the RMSP and RMRJ. This retrieval was important for satellite measurement comparison and correlation analysis with pollutant mean values from ground stations located within our study area.

2.3.3 Ground-based Measurements

NO_2 ground-level concentrations were collected from the State's Environmental Agencies Air Quality Information Systems (CETESB, 2020; INEA, 2020). $PM_{2.5}$ ground measurements were only available from the CETESB Agency. The instrumentation used in both SP and RJ states measures NO_2 by the means of a chemiluminescence method. For $PM_{2.5}$ the standard method is based on Beta radiation absorption.

Both pollutants were gathered in concentration units of $\mu g/m^3$. For NO_2 data, the temporal resolution was in hours, and for $PM_{2.5}$ the values were in daily resolution and defined by the average of 24 hourly samples. In addition, when daily NO_2 was needed, it was defined by the maximum 1-hour value each day.

The ground stations of interest for further statistical analysis were all located within the states metropolitan regions and chosen according to the defined set of criteria detailed below. They are presented in Figures 5 and 6.

- For SP, all stations were within the Water Resources Management Unit nº 6 (WRMU 6) which encompasses the Alto Tiete hydrographic region and is a part of SP's Industrial Vocational Unit (IVU). WRMUs are defined based on "watersheds delimitations, where all marginal water resources converge to a principal waterbody" (CETESB, 2018). For RJ, the stations of interest were within the West Side of the Baia de Guanabara Hydrographic Region.
- For NO_2 in SP, all six selected stations chosen for both data distribution and correlation analysis were active (i.e. measuring pollutant concentrations) throughout all years during 2015-2020. In addition, all of them recorded NO_2 mass concentrations higher than 60

$\mu g/m^3$ at least once for all years. One additional station situated close to a main express highway in Sao Paulo was chosen for additional daily analysis (Marginal Tiete station).

Table 1 – Description of selected ground stations in SP

SP State Stations	Station Location Description
D Pedro II Park	Located between the City's Historical Center and Brás local neighborhood. Cut by five viaducts and the State avenue. D Pedro II Bus Terminal (the busiest in the city), D Pedro II Metro Station and State School of Sao Paulo are within the park area.
Congonhas	Close to Congonhas Airport (busy). Big commerce, hotels and car rental stores. Located about 6 meters of two boulevards, one of which is heavily trafficked with heavy and light duty vehicles, while the other one is not as busy.
Sao Caetano do Sul	Located at a children's municipal, within a residential and industrial region. High income population. High mobile numbers. 753 industries. General (chocolate, toy, ceramics, metal, and mobility industries). Part of ABC Paulista region (highly industrial). General Motors Brazil and two busy boulevards (heavy and light duty vehicles) are nearby.
Cerqueira Cesar	Located within a Public School Faculty and about 7 meters of distance from a heavily trafficked boulevard: heavy and light duty vehicles. Not related to industry emissions.
Pinheiros	Very close to heavy trafficked Marginal Pinheiro highway. Heavy and light duty vehicles. Not related to industry emissions.
Marginal Tiete	Positioned close to main express highway of the city of Sao Paulo. Very busy.

- For NO_2 in RJ, all four selected stations chosen for correlation analysis were located in the Duque de Caxias municipality (DC). Not all of them had available data throughout all study years, for example, the Jardim Primavera station lacked data for 2019. In addition, all the stations miss year 2015. Despite the missing data, these stations were chosen because they were the only ones with enough data to represent a specific area within the hydrographic region in our timeframe. For the boxplot, stations representing not only DC but also the RJ

subregion were chosen because of limitations of data availability throughout years. More details are given under the section Data Limitation (2.4.4.).

Table 2 - Description of selected ground stations in RJ

RJ State Stations	Station Location Description
DC - Campos Eliseos	Petrochemical pole and heavy diesel vehicle traffic nearby. Positioned within small state school.
DC - Jardim Primavera	Very urbanized and also close to heavy diesel vehicle traffic. Positioned within Federal Highway Police area.
DC - Pilar	Close to municipal school and BR-101, a federal busy highway, connecting the entire Eastern Brazil, therefore being highly trafficked.
DC - Sao Bento	Positioned within Municipal Environmental Secretariat, and also close to BR-101.

- For $PM_{2.5}$ in SP, five stations with data constant through the May months of 2015-2020 were chosen for the boxplot. Furthermore, one station close to the main express highway of the city was chosen for more detailed data analysis. The station is the same chosen for NO_2's single station analysis (Marginal Tiete).
- All stations in SP and RJ were situated strategically close to busy highways/boulevards. Therefore, it can be assumed that NO_2 emissions were derived from vehicles. The only exception can be made for the RJ station DC - Campos Eliseos, which is located close to a petrochemical pole that is a potential NO_2 generator.

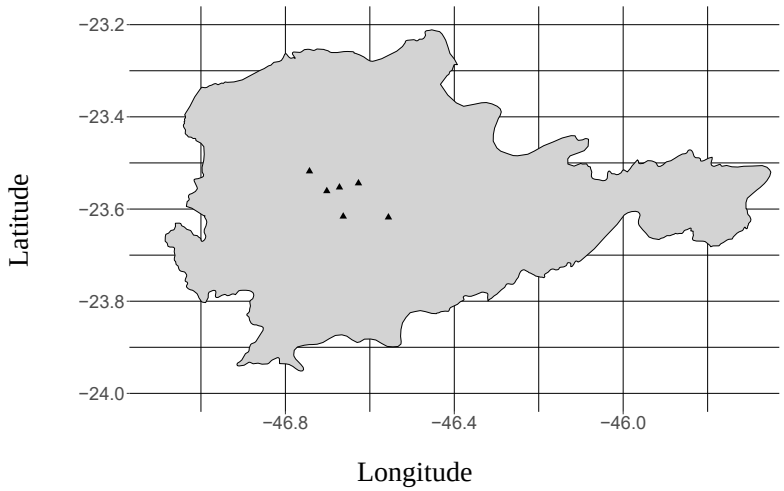

Figure 5 – The six selected ground stations in SP's Alto Tiete Hydrographic Region

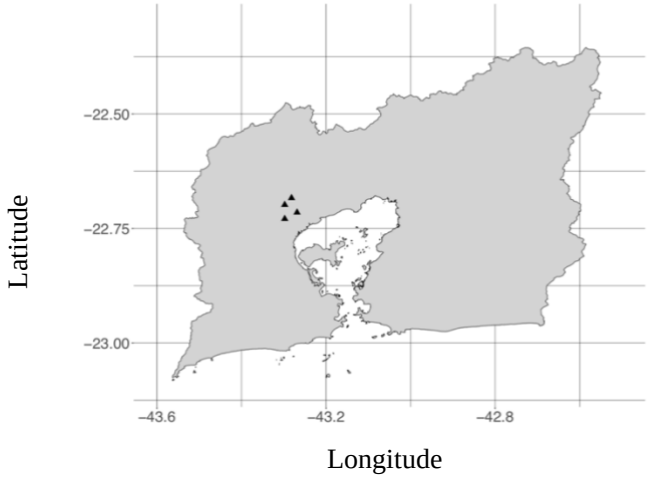

Figure 6 – The four selected ground stations in RJ's Baia de Guanabara Hydrographic Region

2.3.4 Temporal Correlation Analysis

To identify the potential of satellite retrievals to fill up gaps in air pollutant ground-based datasets, a correlation analysis was performed on the collected NO_2 columns and ground concentrations for a timeframe of interest (2015-2020 for SP, and 2016-2020 for RJ). The process can be described in a few steps:

I. Four stations from RJ and six from SP were selected and the respective NO_2 daily measurements averaged for the May month of every year. Then, the final concentrations were converted to volumetric concentrations (ppb).

II. The NO_2 grid column values with the closest latitude-longitude value to the spatial location of the ground station for each year were gathered.

III. The Pearson correlation coefficient between year-to-year changes in ground and column NO_2 was then calculated.

2.4 Results and Discussion

2.4.1 Qualitative Plots

The NO_2 column grids averaged and plotted for the two chosen timeframes resulted in a clear visual distinction in molecule density between the two cases of May 2020 and May 2015-2019 (Figure 7). This was true for both Brazilian states, but more evident in Sao Paulo. The triangles inserted in the plots represent the stations selected for further statistical analysis. From Figure 7a) and 7c), one could notice the stations are positioned in the most polluted area within the Alto Tiete hydrographic region, where the Sao Paulo metropolitan city center is located. On the other hand, RJ stations were not situated in the most concerning area of Baia de Guanabara (where the city and industrial locations are concentrated at). This happened because the ground stations were chosen according to their data availability within years, as detailed in the Materials and Methods section of this document.

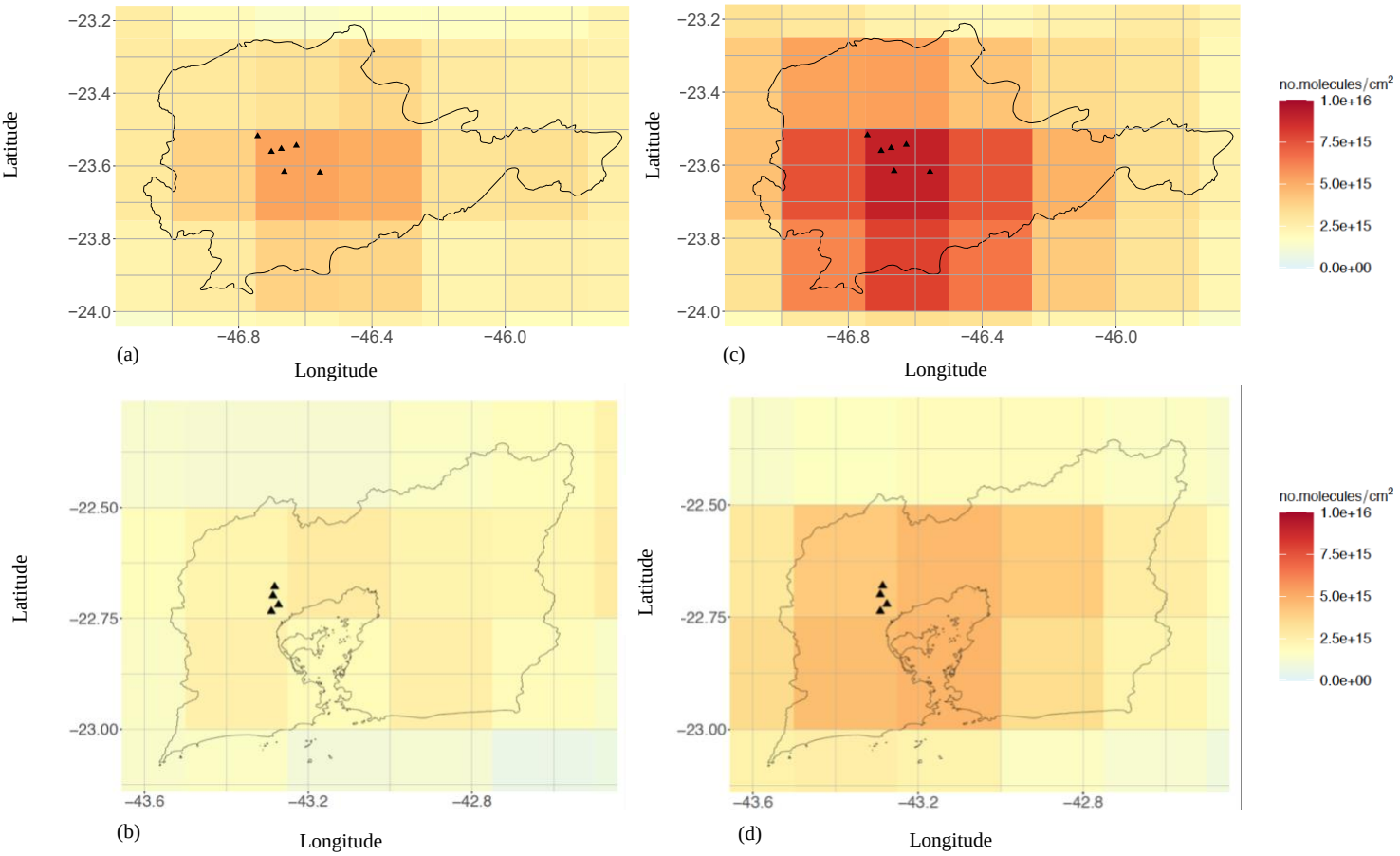

Figure 7- NO_2 column grids in 2020 for SP (7a), RJ (7b); and 2015-2019 for SP(7c), RJ (7d)

2.4.2 Quantitative Analysis

2.4.2.1 OMNO2d Satellite Retrievals

In SP, the range of NO_2 column density values within the hydrographic polygon was $\sim 4.75 \times 10^{15}$ no. molecules/cm^2 (~ 78.83 mol/km^2) for both timeframes (2020 and 2015-2019). This range in the RJ polygon was $\sim 5.28 \times 10^{15}$ no. molecules/cm^2 (~ 87.7 mol/km^2) for 2015-2019, and $\sim 1.75 \times 10^{15}$ no. molecules/cm^2 (~ 29 mol/km^2) for 2020.

The most polluted SP region is located at very busy areas in SP city and its surroundings, including high-income municipalities and the trafficked Congonhas airport. It is also relevant to mention our

SP polygon is situated within the ABC Paulista area, which is characterized as a highly industrial region, where most car manufactories are concentrated in the country. The region presented averaged NO_2 densities of 9.10×10^{15} and 5.28×10^{15} no. molecules/cm^2 in 2015-2019 and 2020, respectively. Therefore, there was a decrease of 42% (3.82×10^{15} no. molecules/cm^2 or 63.45 mol/km^2) in NO_2 column densities when the time span before COVID-19 is compared to the lockdown period. For RJ, the most tainted areas were located close to major roads, and showed pixel densities of 5.28×10^{15} and 2.66×10^{15} no. molecules/cm^2, respectively, for 2015-2019 and 2020. The decrease in this case was of 49.6% (2.62×10^{15} no. molecules/cm^2 or 43.52 mol/km^2) during quarantine.

2.4.2.2 Ground-based Analysis

For the six SP and four RJ selected ground stations, the May month averaged values for each year were transcribed into a boxplot to better understand the observed variations within datasets. NO_2 datasets for 2020 and 2019 were tested and found to follow a standard normal distribution with a difference of light/heavy tails for SP/RJ data, respectively. Furthermore, a student's T-Test was also performed between the same 2020 and 2019 datasets and the difference within monthly means found to be statistically significant for both states assuming a 90% confidence interval with p-values of 0.099 and 0.077 for SP and RJ, respectively.

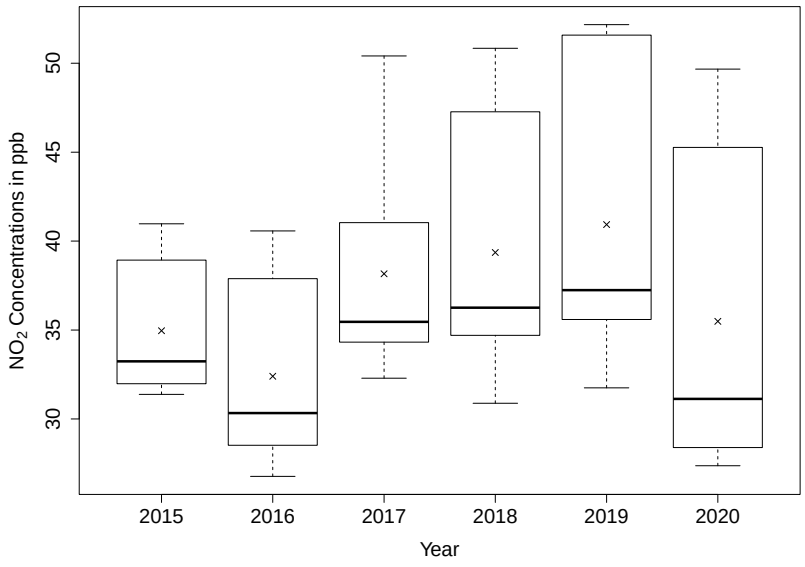

Figure 8 – Yearly boxplots for NO_2 daily ground data over selected SP stations

The crosses on the plots from Figure 8, 9 and 12 represent the average value for the month of May based on daily data from all stations. In addition, the data within the boxes are within the 25% and 75% percentiles, or where 50% of the data values fall at. There was a slight variation in the volumetric NO_2 mean throughout the years, with the highest relative difference observed between 2016 and 2017 (5.76 ppb or 15%) and the second highest between 2019 and 2020 (5.44 ppb or 13.3%). The former disparity was attributed to an unusual favorability in air pollutant dispersion during the winter months (May-September) in the SP State, in accordance to CETEB's 2016 Annual Air Quality Report. The latter difference could be attributed to reduction in traffic due to the local COVID-related lockdown decree. In addition to the annual averages, one might see the range within values was higher for 2018-2020. This can be attributed to high variance within hourly values from the gathered datasets. For a more in-depth analysis, one of the six ground stations was chosen and its yearly values were analyzed.

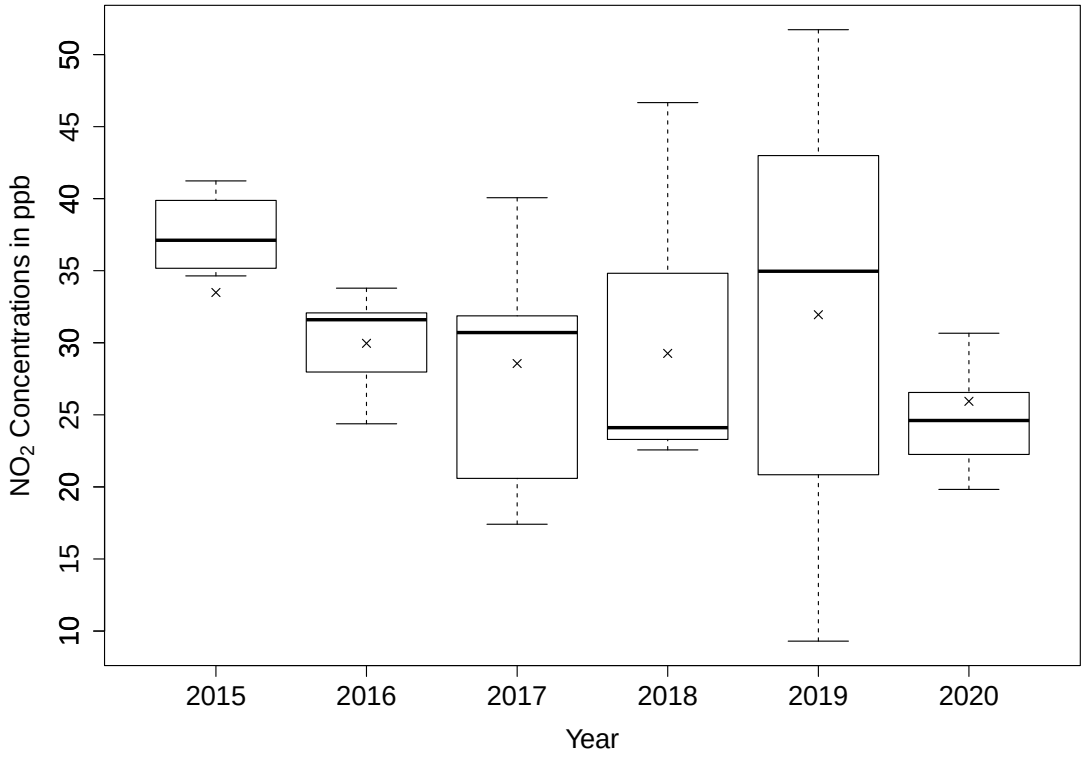

Figure 9 – Yearly boxplots for NO_2 daily ground data over selected RJ stations

Between the 2019 and 2020 years in RJ, the relative deviation in local NO_2 concentrations was 18.8% (6.01 ppb). Results can be seen in Figure 9. The range in stations monthly mean values here was generally smaller here when compared to the SP boxplot. It is also relevant to mention 2019 having a wide range of values for both states, but specifically in RJ this range was higher than in 2020. As with SP, one station was chosen for further statistical analysis.

From the time-series plots presented in Figures 10 and 11, the variations in daily NO_2 concentrations are clear for a single station in each state. The Marginal Tiete SP Station is close to the main express highway in the city, thus potentially capturing high NO_2 levels. There appeared to be a trend in peak levels starting around May 20 and lasting throughout the end of the month. This observation could possibly be related to lower temperatures when winter days are getting colder. Another relevant information extracted from the plot is the relative NO_2 decrease from 2019 to 2020: 5.29 ppb or 15.8%.

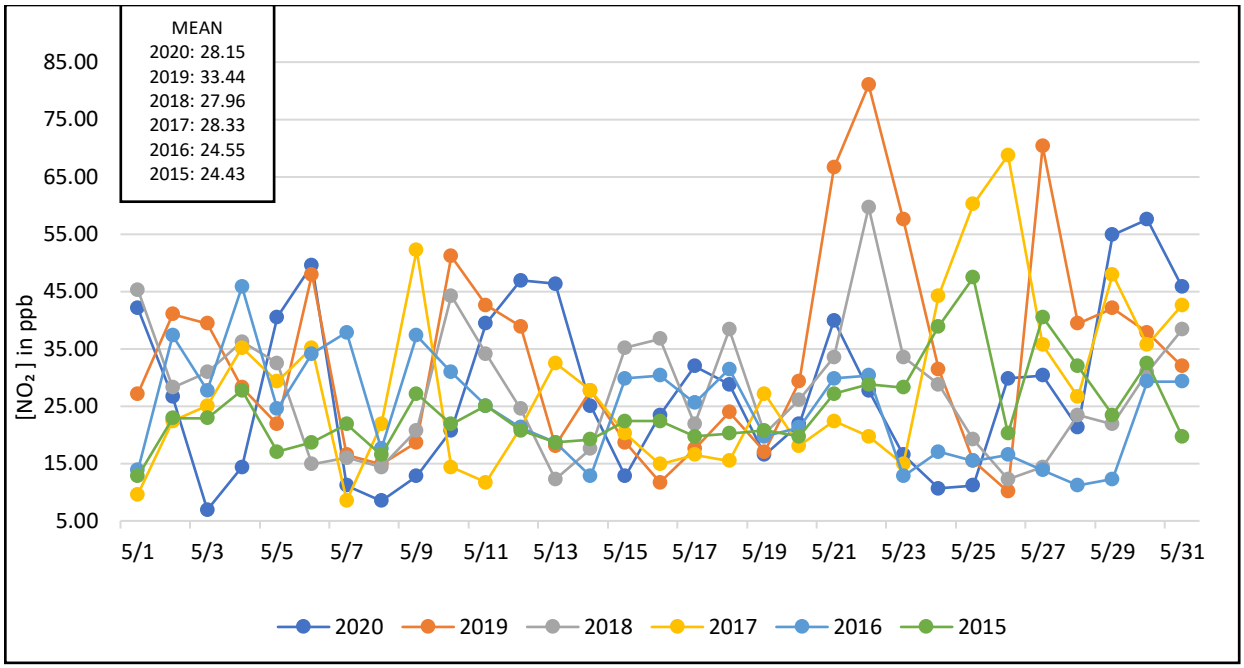

Figure 10 –Daily NO_2 concentrations during 2015-2020 at the Marginal Tiete Station in SP

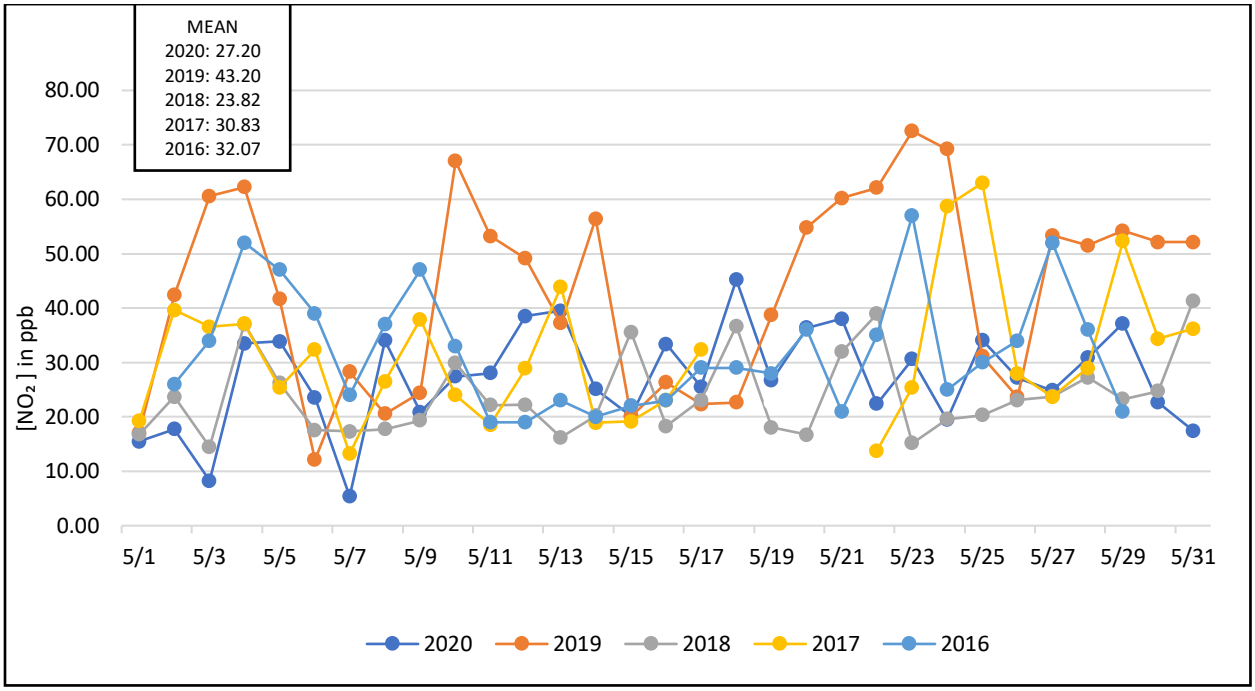

Figure 11 –Daily NO_2 concentrations during 2016-2020 at the DC Pilar Station in RJ

In RJ, the winter season usually begins in June, therefore the seasonality effect should not significantly interfere in NO_2 levels within our timeframe. The decrease for DC's Pilar Station between 2019 and 2020 concentration values was of 16 ppb (37%).

$PM_{2.5}$ ground-level mass concentrations were also evaluated within our timeframe, but only for the SP region since there was no compiled data available for this pollutant at all municipalities of interest in the RJ state.

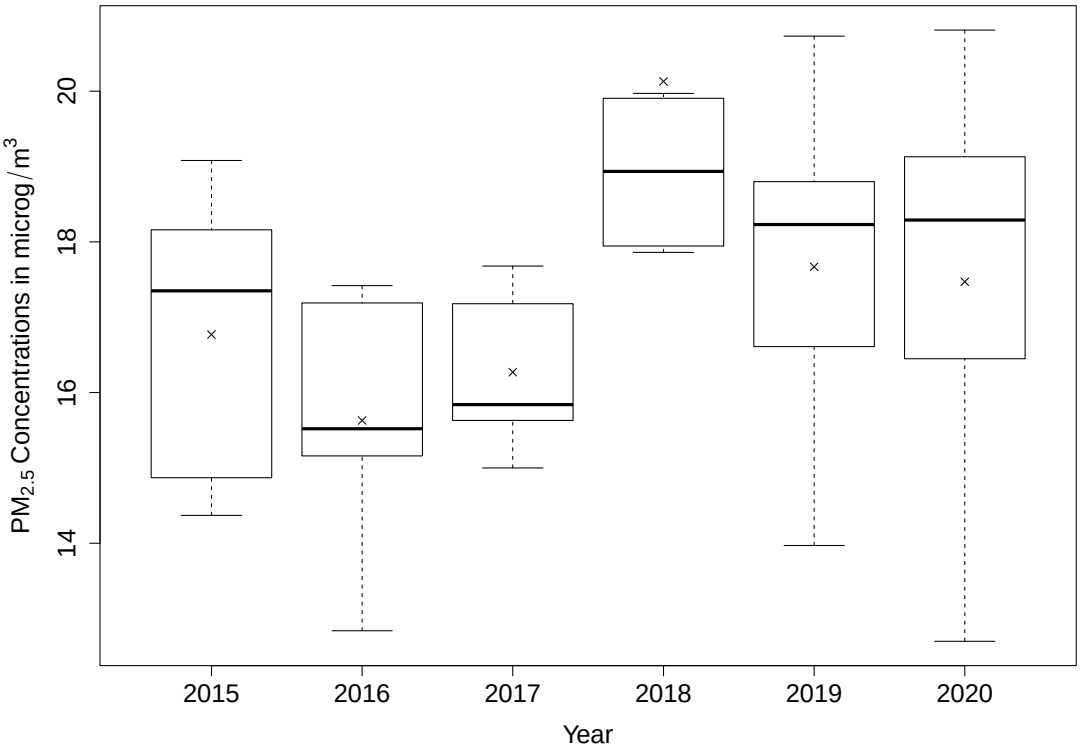

Figure 12 – Yearly boxplots for $PM_{2.5}$ daily ground data over selected SP stations

The selected five $PM_{2.5}$ stations were different than the NO_2 recording sites mainly because not all stations that recorded NO_2 also had $PM_{2.5}$ data available. In addition, some $PM_{2.5}$ stations displayed gaps in daily values for the May month, so only stations with data available for 15 days or more were considered. As shown in Figure 12, there was not a remarkable drop in $PM_{2.5}$ concentrations between 2019 and 2020 (0.2 $\mu g/m^3$ or 0.01%). Nonetheless, in accordance to NO_2 values, the $PM_{2.5}$ mean concentrations fell below the averages in 2016 if all other years are

considered. When a single station was further analyzed, the same trend for all stations in 2016 was observed (see Figure 13). The station chosen was near the Marginal Tiete express highway, and was the same picked for the NO_2 single ground station analysis. However, the values in 2020 were higher compared to 2019 (0.38%). The chosen station is the same as the targeted one for the additional analysis of NO_2.

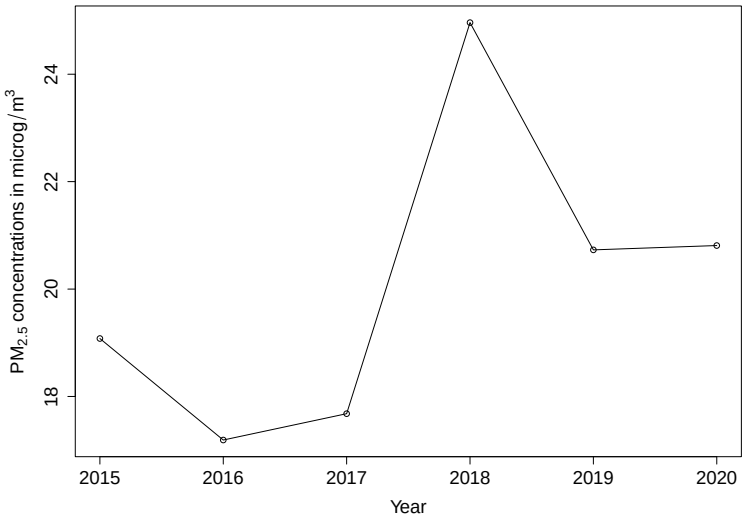

Figure 13 – Yearly mean time-series for $PM_{2.5}$ daily ground data over single SP transport station

2.4.2.3 Correlation Analysis

The yearly mean values of tropospheric NO_2 column densities were retrieved from the grid cells closest to the selected ground stations and are illustrated in the plot below for the SP region of interest.

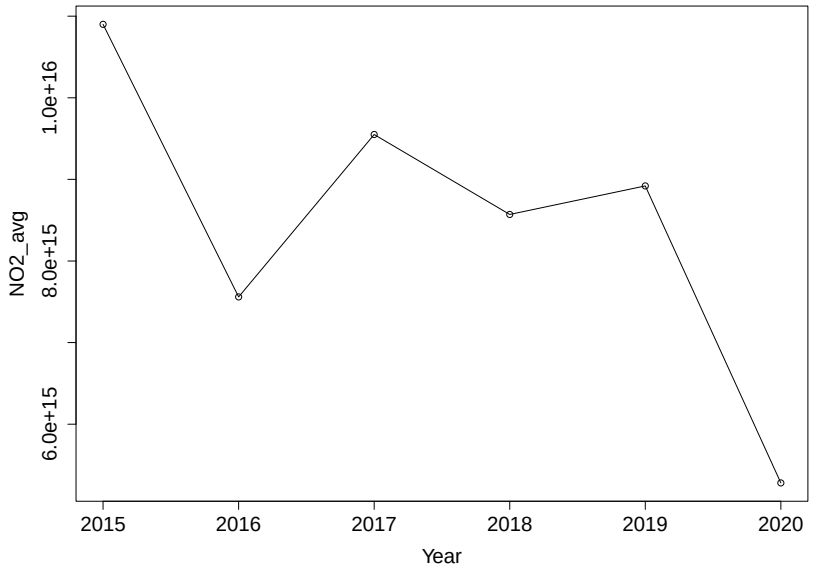

Figure 14– Yearly time-series of mean NO_2 TVCDs over selected SP ground stations

By averaging the 2015-2019 NO_2 values above and comparing the result to the 2020 mean, we found a relative decrease of $\sim$ 42% (or 151 mol/km^2). The Pearson correlation between this dataset and surface data from six SP stations collected between 2 and 3 pm (associated with OMI's local overpassing time) was calculated and a value of 0.77 was obtained.

Table 3 – NO_2 Correlation Data for the SP region

NO_2 measurements/Year	2015	2016	2017	2018	2019	2020
Column Densities Unit: n° molecules/cm^2	1.09E+16	7.56E+15	9.55E+15	8.57E+15	8.92E+15	5.28E+15
Ground-level Unit: ppb	21.54	21.89	24.05	21.82	23.08	16.24
Correlation Coefficient	**0.77**					

For RJ, the yearly NO_2 column densities averages can be observed in Figure 15 below. Here the 2020 mean is 2.21$\times 10^{15}$ no. molecules/cm^2 ($\sim$ 36.71 mol/km^2), and constitutes a decrease of 48.1% from the 2016-2019 mean. Ground concentrations were not available for 2015 from the

chosen stations, so the satellite retrievals were correlated with them beginning in 2016. A Pearson correlation coefficient of 0.53 was found between year-to-year trends of RJ stations and the corresponding satellite column values.

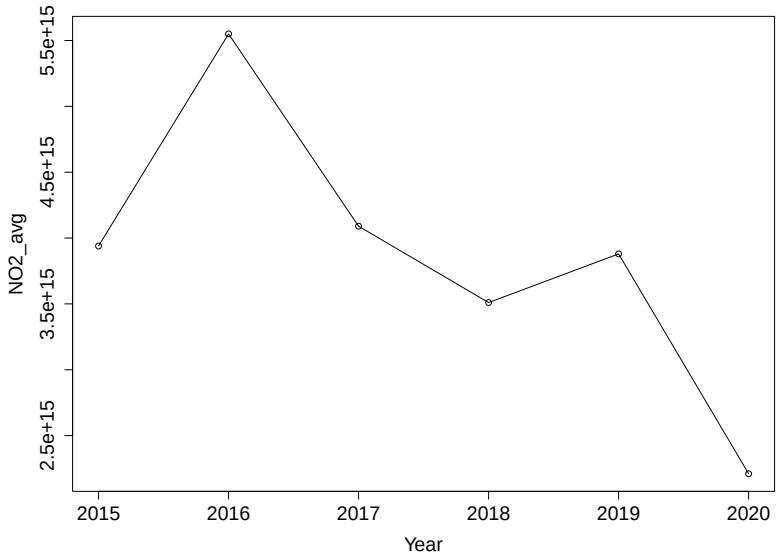

Figure 15 – Yearly time-series of mean NO_2 TVCDs over selected RJ ground stations

Table 4 –NO_2 Correlation Data for the RJ region

NO_2 measurements/Year	2016	2017	2018	2019	2020
Column Densities Unit: n° molecules/cm^2	5.55E+15	4.09E+15	3.51E+15	3.88E+15	2.21E+15
Ground-level Unit: ppb	13.43	13.11	10.01	14.36	11.39
Correlation Coefficient	**0.53**				

2.4.3. Meteorological Conditions and Natural Emissions

From the meteorology reports made available on CETESB's website and additional meteorology data from the Congonhas and Galeao airports (Weather Underground, 2020), it was possible to summarize results regarding air pollutant dispersion conditions in the SP and RJ regions, respectively. The reports gave the number of favorable/unfavorable/unknown number of days for

dispersion within May for each year, however the missing data brought up the need of supplementary information. We followed two of the criteria set by CETESB to define a day with unfavorable conditions for air pollutant dispersion:

I. No rainfall

II. Wind speed < 1m/s

Wind speed data from a busy airport station in SP (Congonhas) was also gathered, and the averaged values above 1 m/s support the report's findings of mostly high number of favorable days for air dispersion within the timeframe (Figure 16).

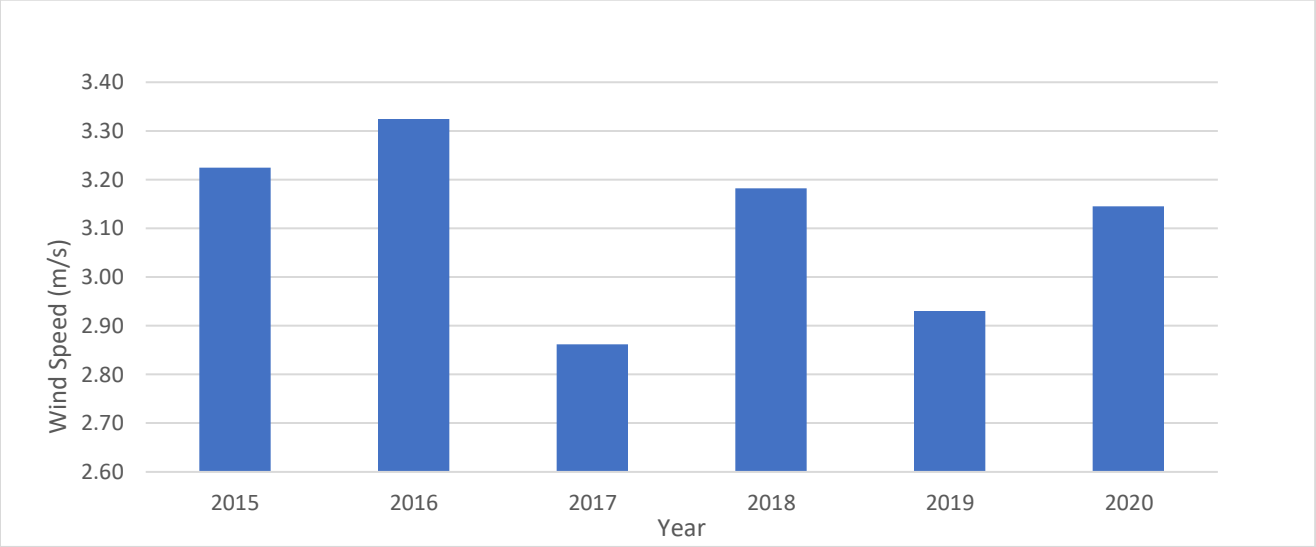

Figure 16 – Daily wind speeds averaged for the May month of 2015-2020 in SP

The averaged air temperatures shown in Figure 17 are also for the Congonhas airport station. The mean seemed to increase more sharply starting from 2016, with a sudden drop in 2020. This 3.03°C decrease, however, did not appear to be significant for any pollutant variations. Yet, it was bigger than the standard deviation of 1.16°C calculated for all years.

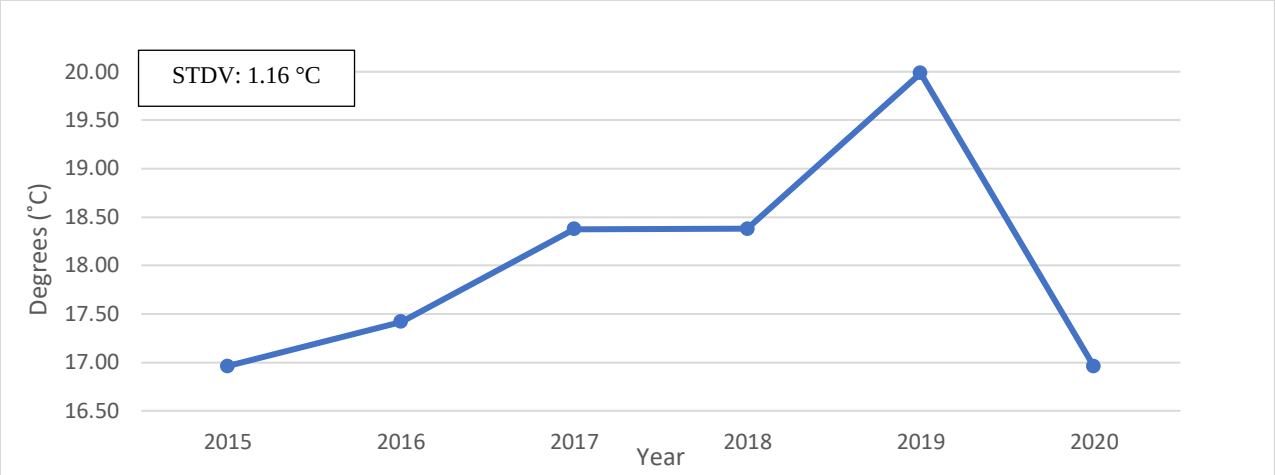

Figure 17 – Yearly mean air temperature for the month of May at selected SP station

For the RJ region, meteorology conditions were also evaluated based on pollutant dispersion parameters and air temperature. The dispersion criteria adopted for the SP findings were also applied here. All daily rainfall data averaged for the May months of 2015-2020 resulted in less than one inch of rainfall, so all values were assumed to be zero. In parallel, daily wind speeds averaged for May were higher than 1 for all years (Figure 18), so it was concluded that all days within our timeframe were favorable to dispersion in RJ.

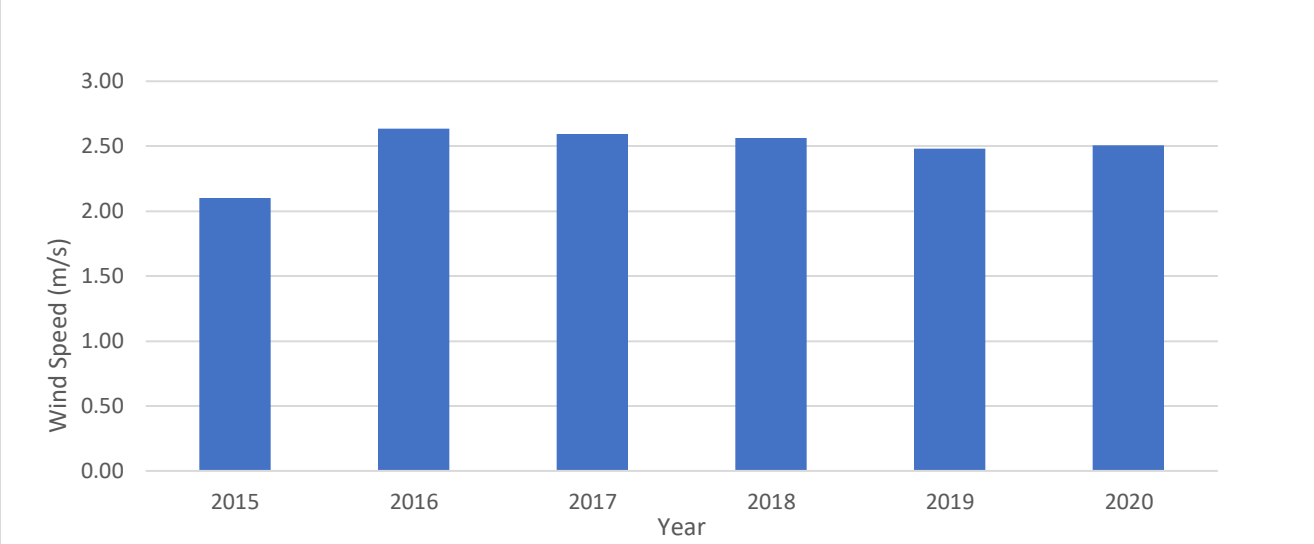

Figure 18 – Daily wind speeds averaged for the May month of 2015-2020 in RJ

According to a single station located at the busiest airport in RJ, temperatures decreased ~ 3°C in 2020 compared to 2019, so no significant effects of temperature were considered to be affecting pollutant levels in the RJ region (Figure 19).

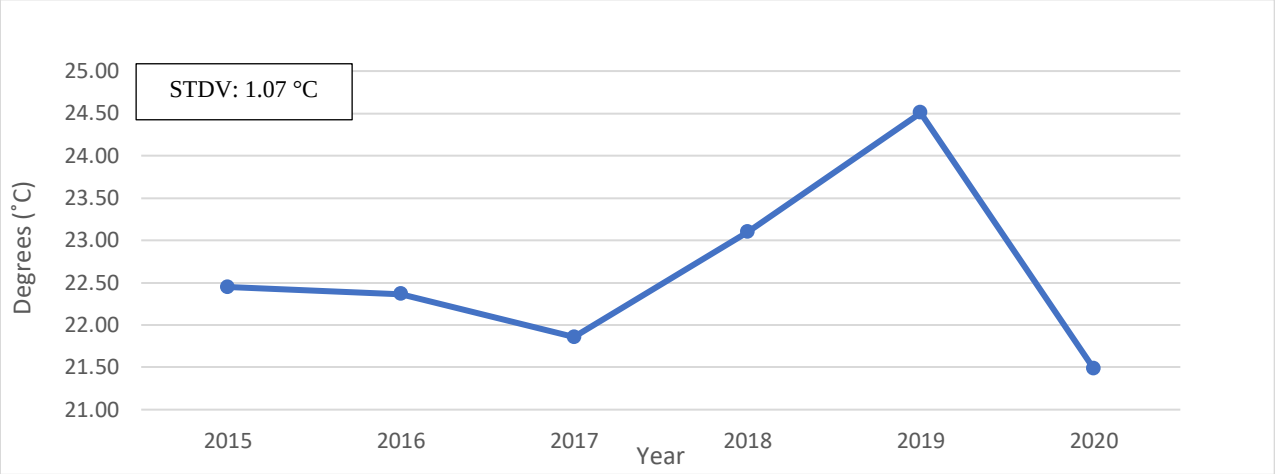

Figure 19 – Yearly mean air temperature for the month of May at selected RJ station

In addition to meteorology parameters, the number of fire hotspots reported by INPE (2020) were also investigated for the Southeast of Brazil, including both states of SP and RJ. The emissions from wildfires are known to contribute to particulate matter and NO_x levels, so we wanted to check if there could be a potential interference of those fire burnings in our yearly data of $PM_{2.5}$ and NO_2.

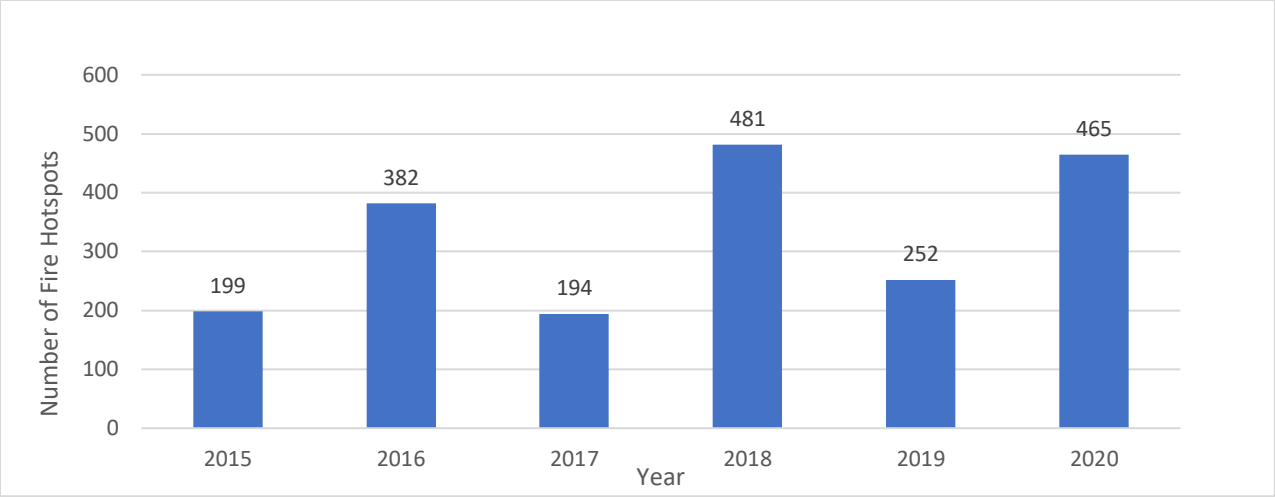

Figure 20 – Number of fire hotspots in Southeast Brazil for the May months of 2015-2020

From Figure 20, the increase in number of fire counts for May 2020 is clear in comparison to the same month in 2019 (~ 46%). Compared to the average count for 2015-2019, the increase in 2020 was ~35%. These results indicate that ground $PM_{2.5}$ and NO_2 values in May 2020 would potentially be higher than in previous years if only wildfires were adding up to these pollutants concentrations. This might be true for $PM_{2.5}$, as we did not see a decrease in 2020 mean values from 2019 during the COVID-19 lockdown period. Furthermore, the distribution of $PM_{2.5}$ values shown in Figure 12 seem to follow the same yearly pattern of the fire counts in the Southeast region, suggesting that the long-range transport of pollutants emitted from fires within Southeastern states could have affected $PM_{2.5}$ values in SP. To support this argument, the following Figure 21 illustrates fire hotspots locations as red dots concentrated in the northwest part of the SP state in 2019. In addition, it was possible to retrieve the dominant wind direction from Wind Finder Portal (2021) at the Congonhas Airport station between 2007 and 2020, which was Southeast. Since most fire hotspots were situated NW, it is logical to assume pollutants originated by the fires (i.e. $PM_{2.5}$) could be transported to the monitoring stations located SE of the hotspots (illustrated as black dots in the Figure 21). In contrast, NO_2 mean values decreased in 2020

compared to 2019 for RJ and SP, and there was no correspondence of yearly distributions with the fire counts.

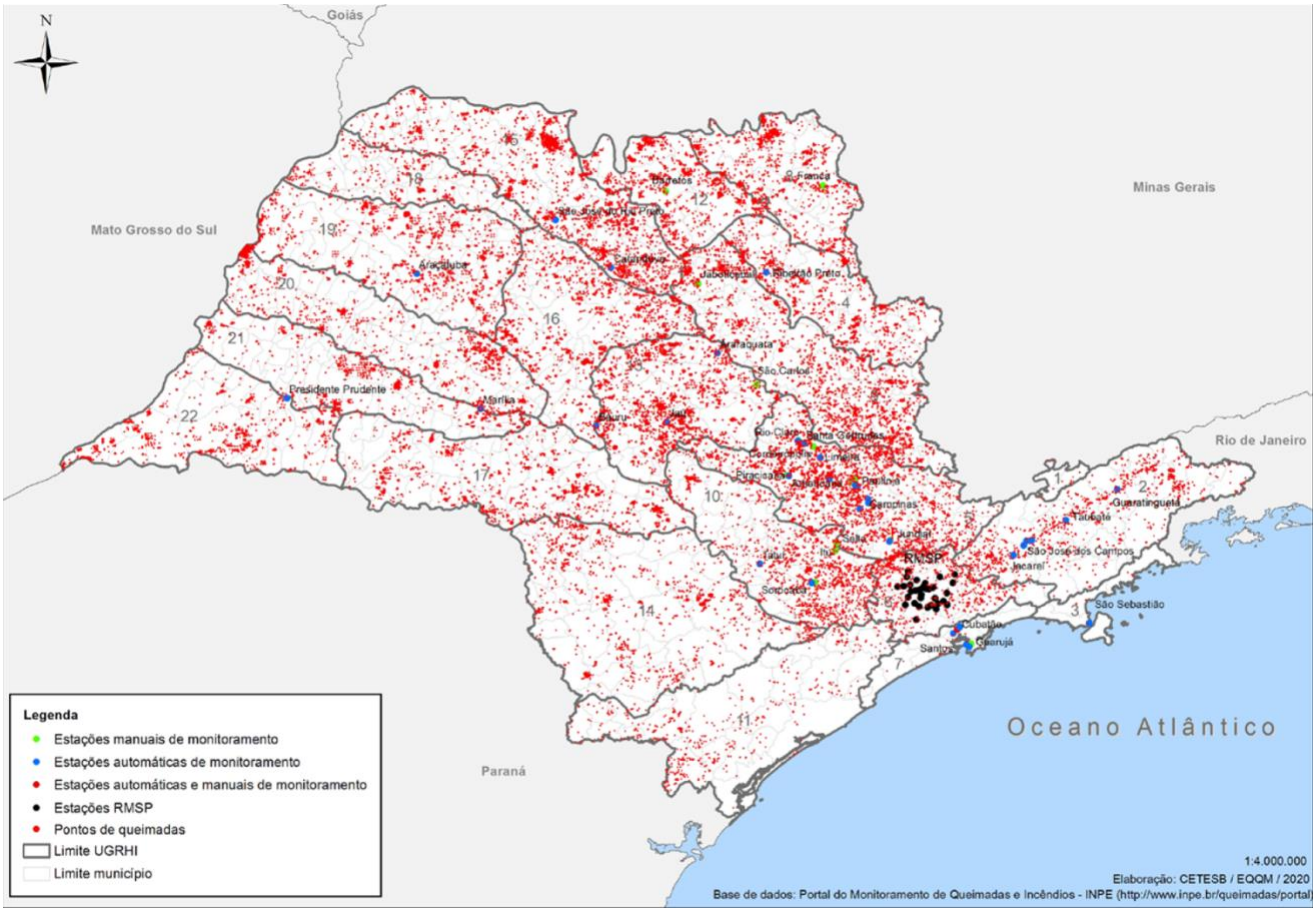

Figure 21 – Monitoring Air Stations and Fire Hotspots within SP state in 2019 (INPE, 2020)

In conclusion, $PM_{2.5}$ in SP was potentially higher in 2020 due to exceeding fire emissions in the Southeast. On the other hand, the NO_2 decrease observed in 2020 did not seem to be influenced by the meteorological/fire factors in both states, since dispersion conditions were similar to previous years, and temperature was slightly but not significantly lower in 2020 for both states.

2.4.4 Data Limitations

Retrieval errors are present when the OMNO2 product is conceived. These include a fitting error in the slant column, estimated to be 0.3 – 1 x 10^{15} no. molecules/cm^2 for all data product levels. In addition, there is a row anomaly (RA) error for Level-1 and 2 data. However, since the grids were created from Level-3 data, the RAs are filtered for the affected cross-track scenes. There are missing values in the daily grid, but since the data was averaged for the whole month of each year, the gaps do not represent a significant error within the product datasets.

Ground data limitations include gaps in daily and hourly concentrations. If the gaps were present in 15 days or more in a month, the correspondent station would be discarded from the analysis. In addition, some hourly values did not have data available, but if there were numbers available for half or more than half of the values within a day, the zeroed values were considered valid and included in the daily averaging. The last relevant limitation in the surface level data was that NO_2 and $PM_{2.5}$ measurements were not available for a fixed set of stations. To be able to choose a set of stations from which data distributions were analyzed in RJ, two regions were defined and varying stations throughout the years were chosen within those regions. In SP, stations were more consistent throughout years, but $PM_{2.5}$ and NO_2 stations did not overlap except for the Marginal Tiete, Congonhas stations.

2.5 Conclusions

Qualitative and quantitative differences in NO_2 and $PM_{2.5}$ concentrations were investigated for timeframes before and during the COVID-19 lockdown imposed by the Brazilian government. To analyze if there were any significant differences in NO_2 and $PM_{2.5}$ concentrations in 2020 during lockdown compared to previous years, satellite and ground-based measurements were synergistically analyzed. After finding a clear visual difference in gridded NO_2 column densities

for the month of May in 2015-2019 and 2020 within the hydrographic regions of interest (where the selected ground stations were located), a quantitative analysis was executed. From OMI satellite retrievals, we found a decrease of 42% in 2020 compared to the 2015-2019 period in SP's Alto Tiete. An even higher decline of 49.6% was found in RJ's Baia de Guanabara for the same time interval.

Aside from satellite NO_2 columns, ground concentrations also presented differences within years. Yet, the difference seemed to be smaller than that for satellite retrievals. In May 2020, NO_2 levels were 13.3% lower (p-value = 0.099 than for the same month in 2019 for SP, while in RJ this drop was equal to 18.8% (p-value = 0.077) in 2020. Although this difference was higher in RJ, the concentrations in 2019 had a high range within local selected stations. The lowest range value was associated with DC's São Bento station, and the highest was at RJ's Manguinhos station. For SP and RJ transportation stations, the NO_2 drop was also present in 2020, and still higher for the RJ region. $PM_{2.5}$ mass concentrations did not show a significant contrast between 2019 and 2020 neither for multiple nor single stations.

The correlation coefficients between year-to-year trends of satellite column NO_2 and ground-based measurements for multiple selected stations were ~0.77 for SP and ~0.53 for RJ.

To examine if there was any weather interference on the statistical comparison performed on this study, the dispersion conditions and mean air temperature for selected stations were studied for SP and RJ. Both SP and RJ stations showed mostly favorable dispersion days for all days during the month of May in all years, so this factor was not considered to be affecting the NO_2 decrease found for 2020. Furthermore, natural emissions by wildfire were examined using the number of hotspots within the Southeast region, and it was concluded that $PM_{2.5}$ concentrations were potentially being affected by those fires.

2.6 Acknowledgments

This research was supported by the Virginia Polytechnic Institute and State University. The authors thank the Brazilian Environmental Agencies, Companhia de Tecnologia Ambiental do Estado de Sao Paulo (CETESB-SP) and Instituto Estadual do Ambiente (INEA-RJ) for providing the ground-based data.

References

Andrade, M. et al. "Vehicle emissions and PM2.5 mass concentrations in six Brazilian cities". *Air Quality, Atmosphere and Health* 5 (2012): 79-88. doi: 10.1007/s11869-010-0104-5.

Bechle, M., Millet D., Marshall, J. "Remote sensing of exposure to NO2: Satellite versus ground-based measurement in a large urban area". *Atmospheric Environment* 69 (2013): 345-353. doi.org/10.1016/j.scitotenv.2020.141820.

Berman, J., and Ebisu, K. "Changes in U.S. air pollution during the COVID-19 pandemic". *Science of the Total Environment* 739 (2020): doi.org/10.1016/j.scitotenv.2020.139864.

Croda, J. et al. "COVID-19 in Brazil: advantages of a socialized unified health system and preparation to contain cases". *Revista da Sociedade Brasileira de Medicina Tropical*. 53 (2020): ISSN 1678-9849. doi.org/10.1590/0037-8682-0167-2020.

Dantas, G. et al. "The impact of COVID-19 partial lockdown on the air quality of the city of Rio de Janeiro, Brazil". *Science of the Total Environment* 729 (2020): doi.org/10.1016/j.scitotenv.2020.139085.

Duncan, B. et al. "Satellite data of atmospheric pollution for U.S. air quality applications: Examples of applications, summary of data end-user resources, answers to FAQs, and

common mistakes to avoid". *Atmospheric Environment* 94 (2014): 647-662. doi.org/10.1016/j.atmosenv.2014.05.061.

Ghahremanloo, M., Lops, Y., Choi, Y. "Impact of the COVID-19 outbreak on air pollution levels in East Asia". *Science of the Total Environment* 754 (2021): doi.org/10.1016/j.scitotenv.2020.142226.

Hodan, W., and Barnard, W. "Evaluating the Contribution of PM 2.5 precursor gases and re-entrained road emissions to mobile source PM 2.5 Particulate Matter Emission". *MACTEC Under Contract to the Federal Highway Administration* (2004). MACTEC Federal Programs, Research Triangle Park, NC.

Hu, X. et al. (2017). "Estimating PM 2.5 Concentrations in the Conterminous United States Using the Random Forest Approach". *Environmental Science and Technology* 51 (12) (2017): 6936–6944. doi.org/10.1021/acs.est.7b01210.

Instituto Nacional de Pesquisas Espaciais - INPE. Burning and Fire Monitoring Portal. Acessed: December 1, 2020. http://www.inpe.br/queimadas.

Krotkov, N., et al. The version 3 OMI NO2 standard product. *Atmospheric Measurement Techniques Discussion*, in review, 2017. doi:10.5194/amt-2017-44.

Krotkov, N., et al. OMI/Aura NO2 Cloud-Screened Total and Tropospheric Column L3 Global Gridded 0.25 degree x 0.25 degree V3. NASA Goddard Space Flight Center: Goddard Earth Sciences Data and Information Services Center (GES DISC), 2019. Accessed March 3rd, 2020. 10.5067/Aura/OMI/DATA3007/.

Kumar, S. "Effect of meteorological parameters on spread of COVID-19 in India and air quality during lockdown". *Science of the Total Environment* 745 (2020): doi.org/10.1016/j.scitotenv.2020.141021.

Liu, Q. et al. “Spatiotemporal impacts of COVID-19 on air pollution in California, USA”. *Science of the Total Environment* 750 (2021): doi.org/10.1016/j.scitotenv.2020.141592.

Lovric, M. et al. “Understanding the true effects of the COVID-19 lockdown on air pollution by means of machine learning”. *Environmental Pollution* 269 (2020): Article 115900. doi.org/10.1016/j.envpol.2020.115900.

Nakada, L., and Urban, R. “COVID-19 pandemic: Impacts on the air quality during the partial lockdown in São Paulo state, Brazil”. *Science of the Total Environment* 730 (2020): doi.org/10.1016/j.scitotenv.2020.139087.

Oner, E., and Kaynak, B. “Evaluation of NOx emissions for Turkey using satellite and ground-based observations”. *Atmospheric Pollution Research* 7 (2016): Issue 3, 419-430. doi.org/10.1016/j.apr.2015.10.017.

Petritoli, A. et al. “First comparison between ground-based and satellite-borne measurements of tropospheric nitrogen dioxide in the Po basin”. *Journal of Geophysical Research* 109 (2004): D15307. doi:10.1029/2004JD004547.

Rio de Janeiro State Institute of the Environment– INEA. QUALIAR: Air Quality and Meteorology Information System. Accessed March 3rd, 2020. http://200.20.53.25/qualiar/home/index.

Rio de Janeiro State Institute of the Environment– INEA. “Relatório da Qualidade do Ar do Estado do Rio de Janeiro – Ano Base 2015”. Rio de Janeiro: INEA, 2015.

Rivera, C., Stremme, W., Grutter, M. “Nitrogen dioxide DOAS measurements from ground and space: comparison of zenith scattered sunlight ground-based measurements and OMI data in Central Mexico”. *Atmósfera* 26 (2013): Issue 3, 401-414. doi.org/10.1016/S0187-6236(13)71085-3.

São Paulo State Environmental Agency – CETESB. “Qualidade do ar no estado de São Paulo 2018”. São Paulo: CETESB, 2019.

São Paulo State Environmental Agency – CETESB. QUALAR: Air Quality Information System. Accessed March 3rd, 2020. https://qualar.cetesb.sp.gov.br/qualar/home.do.

Shen, L. et al. “Importance of meteorology in air pollution events during the city lockdown for COVID-19 in Hubei Province, Central China”. *Science of the Total Environment* 754 (2021): doi.org/10.1016/j.scitotenv.2020.142227.

Siciliano, B. et al. “Increased ozone levels during the COVID-19 lockdown: Analysis for the city of Rio de Janeiro, Brazil”. *Science of the Total Environment* 737 (2020): doi.org/10.1016/j.scitotenv.2020.139765.

Siciliano, B. et al. “The impact of COVID-19 partial lockdown on primary pollutant concentrations in the atmosphere of Rio de Janeiro and Sao Paulo megacities (Brazil)”. *Bulletin of Environmental Contamination and Toxicology* 105 (2020b): 2-8. doi.org/10.1007/s00128-020-02907-9.

Tobías, A. et al. “Changes in air qualiy during the lockdown in Barcelona (Spain) one month into the SARS-CoV-2 epidemic”. *Science of the Total Environment* 726 (2020): doi.org/10.1016/j.scitotenv.2020.138540.

Transportation Research Board. “The Congestion Mitigation and Air Quality Improvement Program, assessing 10 years of experience”. *Special Report* (2002): 60-4. Washington, DC: Transportation Research Board, National Research Council.

Volten et al. “NO2 Lidar profile measurements for satellite interpretation and validation”. *Journal of Geophysical Research: Atmospheres* 114 (2009): Issue D24. 10.1029/2009JD012399.

U.S. EPA: Environmental Protection Agency. "Criteria Air Pollutants". Last updated on November 17, 2020. Accessed December 2, 2020. https://www.epa.gov/criteria-air-pollutants/.

Yuan, Q. et al. "Spatiotemporal variations and reduction of air pollutants during the COVID-19 pandemic in a megacity of Yangtze River Delta in China". *Science of the Total Environment* 751 (2021): doi.org/10.1016/j.scitotenv.2020.141820.

Wang, C. et al. "Comparison and Validation of TROPOMI and OMI NO2 Observations over China". *Atmosphere* 11 (2020): 363. doi:10.3390/atmos11060636.

Weather Underground. Weather Underground Sao Paulo Congonhas Station, Brazil History Data. Accessed December 1, 2020. https://www.wunderground.com/history/monthly/br/s%C3%A3o-paulo/SBSP/date/2020-5.

Weather Underground. Weather Underground Rio de Janeiro Galeao Station, Brazil History Data. Accessed December 1, 2020. https://www.wunderground.com/history/monthly/br/s%C3%A3o-paulo/SBSP/date/2020-5.

WHO. "2019-nCoV outbreak is an emergency of international concern". January 2020. Accessed in December 6, 2020. http://www.euro.who.int/en/health-topics/health-emergencies/international-health-regulations/news/news/2020/2/2019-ncov-outbreak-is-an-emergency-of-international-concern/.

WHO/Europe. Statement on the second meeting of the International Health Regulations (2005). Accessed in December 6, 2020. Emergency Committe regarding the outbreak of novel coronavirus (2019-nCov). https://www.who.int/news-room/detail/30-01-2020-

statement-on-the-second-meeting-of-the-international-health-regulations-(2005)-emergency-committee-regarding-the-outbreak-of-novel-coronavirus-(2019-ncov)/.

Windfinder. Wind Finder Portal. Accessed in January 1, 2021. https://pt.windfinder.com/.

Zhao, Y. et al. “Substantial changes in Nitrogen Dioxide and Ozone after excluding meteorological impacts during the COVID-19 outbreak in Mainland China”. *Environmental Science and Technology Letters* 7 (2020): 402-408. doi.org/10.1016/j.scitotenv.2020.141592.

Chapter 3. Conclusions

3.1 Conclusions

Performing side-by-side statistical comparisons and correlations between NO_2 satellite retrievals and the corresponding surface air pollutant datasets are useful to bring up the potential that satellite instruments have in capturing column densities, especially when there are not enough ground-based data being measured in a region of interest. This can be applied in different cases studies, but here we aimed to evaluate the air quality situation with respect to NO_2 and $PM_{2.5}$ before and during the COVID-19 lockdown timeframe in two Brazilian states.

The hydrographic regions in the Sao Paulo and Rio de Janeiro states that encompassed the busiest metropolitan regions in both places were chosen to be analyzed. For Sao Paulo this region was Alto Tiete, and for Rio it was Baia de Guanabara. Industrial activity was not generally affected by the lockdown measures, but there were limitations imposed on vehicle circulation. The resulted change in NO_2 concentrations were hereby analyzed using satellite column and surface measurements. This criteria air pollutant was chosen because it is mostly emitted from vehicles and it is short-lived in the atmosphere. $PM_{2.5}$ was also evaluated at the ground level since it can also be emitted from vehicles and can be associated with several adverse health effects. Fine particles can also significantly reduce visibility.

By plotting the NO_2 column grid, qualitative differences in concentration levels before and during quarantine were observed for the May months of the chosen timeframes in both study areas. Following with quantitative analysis, a 42% decrease of NO_2 columns was found in SP for 2020, in comparison to 2015-2019. For six SP stations, the ground-level NO_2 reduction in 2020 was 13.3% (p-value = 0.099) compared to 2019. The correlation coefficients between year-to-year trends of satellite and ground measurements was approximately 77%. In RJ, the NO_2 column

reduction in 2020 was 49.6% compared to 2015-2019. Surface data for the same pollutant showed a reduction of around 18.8% (p-value = 0.077) in 2020 from the previous year. The correlation between satellite and ground trends in RJ was about 53% for the stations of interest. No significant reduction was found in $PM_{2.5}$ compared to the previous year.

Finally, since air pollutant levels tend to be influenced by weather conditions and natural emissions, an effort was made to study local weather characteristics and wildfire hotspots within our timeframe to detect if there was any interference of those in our pollutant comparison analysis. Data on rainfall, temperature, wind speed, and number of fire hotspots were analyzed for this purpose. Daily rainfall was less than one inch for all days in all years within the two states. The mean air temperature at the SP and RJ stations was ~3 °C lower in 2020 compared to 2019, not considered significant enough to affect the difference found between pollutant levels for the same timeframe having in mind the temperature standard deviation in both states was between 1-1.2 °C. With that and after looking into wind speed data, it was concluded that mean NO_2 and $PM_{2.5}$ pollutant levels in SP and RJ were not generally affected by dispersion conditions in 2020, and the decrease found for NO_2 satellite and ground-based data was indeed derived from COVID-19 lockdowns. Nevertheless, a similarity was observed between the year-to-year trends of $PM_{2.5}$ and number of wildfire hotspots throughout the years. For the Southeast region of Brazil, there were 46% more fire hotspots in May 2020 compared to the same month in 2019, while $PM_{2.5}$ concentrations showed a drop of only 0.01% between the same time period at the SP stations of interest. This result shows a potential reason why $PM_{2.5}$ did not present lower concentrations in May 2020: long-range transport of the pollutant from a higher number of fire hotspots when the same month in 2019 is taken in consideration.

In conclusion, this research work was useful not only to evaluate NO_2 and $PM_{2.5}$ concentrations before and during COVID-19 lockdown in Southeast Brazil regions, but also the potential of satellite retrievals to perform such comparisons and serve as a reference for NO_2 concentrations. On the present study, the 2015 NO_2 column measurements for RJ could possibly be used to estimate ground concentrations at the respective RJ region of interest, since no surface measurements were available there. It is known that air pollutant ground measurement stations in Brazil are not equally distributed: in fact, they tend to be very sparse and limited in number throughout the country. Thus, satellite retrievals become important alternatives when missing data is present in surface datasets or when stations are not available.

3.2 Recommendations for Future Work

For future studies, we suggest taking advantage of TROPOMI retrievals, as OMI is soon to be discontinued and TROPOMI has nine times the spatial resolution that OMI provides in addition to better data homogeneity (Wang et al., 2020).

In addition to other satellite instrumentation, it is also recommended that alternative remote sensing devices, such as Lidars, are used for NO_2 retrievals to better and more closely compare vertical columns with ground-based results. The use of a mobile Lidar system is described by Volten et al. (2009).

Furthermore, subsequent studies should recur to weather-normalization or machine learning techniques, such as the random forest model (RFM), to evaluate pollutant concentration tendencies for large sets of data and do not base their results solely on pollutant surface measurements. This was done in recent studies such as in Austria (Lovric M. et al. (2020), where the predicted (expected) and observed (true) pollution levels were evaluated based on local environmental data

of NO_2, PM_{10}, O_3 and O_x. Another application of RFM was used in Hu et al. (2017) for $PM_{2.5}$ concentration estimations in the Conterminous U.S.

APPENDIX A – Additional Satellite Systems Information

By the means of this appendix, descriptions of current relevant satellite systems are made available. These machines include, but are not limited to:

I. TERRA is located at a circular sun-synchronous polar orbit that takes it from north to south (on the daylight side of the Earth) every 99 minutes. *Launched in December 18, 1999.*

II. Suomi NPP is in a sun-synchronous near-circular polar orbit (of the primary NPP), altitude = 824 km, inclination =98.74º, period = 101 minutes, LTDN (Local Time on Descending Node) at 10:30 hours. The repeat cycle is 16 days (quasi 8-day). *Launched in October 28, 2011.*

III. Aura was launched into a sun-synchronous, near polar (98.2 degree inclination) orbit. It orbits 705 km (438 miles) above the Earth with a sixteen-day repeat cycle and 233 revolutions per cycle. The ascending node is in daylight and crosses the equator at approximately 1:45 PM. The Aura spacecraft is flying in formation with other Earth observing satellites called the A-Train. *Launched in July 15 2004.*

IV. Aqua circles the Earth every 99 minutes and is in a polar orbit, passing within ten degrees of each pole on every orbit. The orbit is sun-synchronous, meaning that the satellite always passes over a particular part of the Earth at about the same local time each day. Aqua always crosses the equator from south to north at about 1:30 PM local time. *Launched in May 4 2002.*

V. Sentinal-5 is in a sun-synchronous low earth orbit with a mean altitude of 817 km with a descending node crossing of 09:30 AM mean local solar time for the MetOp-SG A satellites. In a sun-synchronous orbit, the surface is illuminated at roughly the same sun

angle each time the satellite passes overhead. A high inclination orbit (approximately 98.7°) is used. The orbit inclination is the angular distance of the orbital plane from the equator. The orbital cycle is 29 days (14 orbits per day, 412 orbits per cycle). The orbit cycle is the time taken for the satellite to return over the same geographical point on the ground with the same viewing geometry. *Launched in October 13 2017.*

VI. CALIPSO flies as part of the Aqua satellite constellation (or A-Train), which consists of the Aqua, CloudSat, CALIPSO, PARASOL, and Aura satellite missions. The constellation has a nominal orbital altitude of 705 km and inclination of 98 degrees. Aqua will lead the constellation with an equatorial crossing time of about 1:30 PM. CloudSat and CALIPSO lag Aqua by 1 to 2 minutes and will be separated from each other by 10 to 15 seconds. *Launched in April 2006.*

VII. The International Space Station maintains an orbit with an average altitude of 400 kilometers (250 mi). It circles the Earth in roughly 92 minutes and completes 15.5 orbits per day. *Launched in November 1998.*

APPENDIX B – Additional Satellite Instruments Information

Further definitions on different satellite instruments available from NASA's Earth Data Remote Sensor webpage[1] can be found below. In addition to those, examples and specifications for each sensor are mentioned.

Adapted and retrieved definitions from NASA's Earth Data Remote Sensor webpage:

I. LIDAR**:** light detection and ranging sensor that uses a laser (light amplification by stimulated emission of radiation) radar to transmit a light pulse and a receiver with sensitive detectors to measure the backscattered or reflected light. Distance to the object is determined by recording the time between transmitted and backscattered pulses and by using the speed of light to calculate the distance traveled.

   i. CALIOP: provides high-resolution vertical profiles of *aerosols and clouds* through one channel receiving backscattered light in 1064 nm and two other channels receiving light in the 532 nm range. A table summarizing its technical details can be found below.

II. Imaging Radiometer: non-scanning imager used to improve spatial and height resolution with measurements of radiation intensity over the maximum possible optical field of view. It is nadir-viewing (observes the atmosphere by looking straight down) and has a 64x64 km swath that produces images with a pixel size of 1 km. They work in different wavelengths than the CALIOP LIDAR: thermal infrared region at 8.7, 10.5 and 12 micrometers. Those wavelengths were selected

[1]What is Remote Sensing?" NASA's Earth Data: Open Access for Open Science. Last updated on Nov 17, 2020. Accessed December 02, 2020. https://earthdata.nasa.gov/learn/backgrounders/remote-sensing/.

to optimize CALIPSO retrievals of cirrus cloud emissivity and particle size. A table summarizing its technical details can be found below.

i. VIIRS: collects global satellite observations that span the visible and infrared wavelengths across land, ocean, and atmosphere. A whiskbroom radiometer by design, it has 22 channels ranging from 0.41 μm to 12.01 μm. For more specifications, consult https://ladsweb.modaps.eosdis.nasa.gov/missions-and-measurements/viirs/.

III. Imaging Spectroradiometer: measures the intensity of radiation in multiple wavelength bands (i.e., multispectral). Many times the bands are of high-spectral resolution, designed for remotely sensing specific geophysical parameters.

i. MODIS: provides high radiometric sensitivity (12 bit) in 36 spectral bands ranging in wavelength from 0.4 μm to 14.4 μm. Two bands are imaged at a nominal resolution of 250 m at nadir, with five bands at 500 m, and the remaining 29 bands at 1 km. A ±55-degree scanning pattern at the EOS orbit of 705 km achieves a 2,330-km swath and provides global coverage every one to two days. For more specifications, consult https://modis.gsfc.nasa.gov/about/specifications.php.

ii. MIRS: has 9 built-in cameras that provide 5 different viewing angles. This setting achieves higher scattering angle coverage, which means enhanced sensitivity to atmospheric aerosol effects and to cloud reflectance effects. In each of the nine MISR cameras, images will be obtained in four spectral bands, i.e. in four different colors, one each for

blue, green, red, and near-infrared. The center wavelength of each of these bands is 446, 558, 672, and 867 nanometers respectively. During each orbit, MISR obtains a swath of imagery that is 360 km wide by about 20,000 km long. For more specifications, consult https://misr.jpl.nasa.gov/Mission/misrInstrument/.

IV. Imaging Spectrometer: designed to detect, measure, and analyze the spectral content of incident electromagnetic radiation. Conventional imaging spectrometers use gratings or prisms to disperse the radiation for spectral discrimination.

i. MODIS: provides high radiometric sensitivity (12 bit) in 36 spectral bands ranging in wavelength from 0.4 μm to 14.4 μm. Two bands are imaged at a nominal resolution of 250 m at nadir, with five bands at 500 m, and the remaining 29 bands at 1 km. A ±55-degree scanning pattern at the EOS orbit of 705 km achieves a 2,330-km swath and provides global coverage every one to two days. For more specifications, consult https://modis.gsfc.nasa.gov/about/specifications.php.

ii. OMI: has two built-in imaging spectrometers that detects molecular absorption of the Visible and UV wavelengths part of the electromagnetic spectrum: 350-500nm for visible and 270-314 nm for UV1, and 306-380 nm for UV2. Its ground resolution is 13x25 km and spectral resolution is 1-0.45 nm FWHM. Its duty cycle is 60 minutes on daylight side, with daily global coverage. It is a nadir-viewing wide-field instrument. For more specifications, consult https://aura.gsfc.nasa.gov/omi.html.

iii. TROPOMI: measures the lower part of the atmosphere: the troposphere. It has four detectors that can measure wavelengths in infrared, visible and UV wavelengths one more wavelength range than OMI instruments – infrared). The Tropomi detector takes a picture of the earth every second as it glides underneath it. The entire detector has an image area of 2,600 by 7 kilometers. Each pixel on the detector covers a piece of earth surface of 7 × 7 kilometers. Tropomi can therefore assess air quality at the level of cities. For more specifications, consult https://www.knmi.nl/kennis-en-datacentrum/uitleg/tropomi.

iv. OMPS: next-generation of back-scattered UV (BUV) radiation sensors. It provides well calibrated measurements from two nadir sensors (one focused on total column ozone retrieval and one focused on ozone profile retrieval) and a sensor looking at the atmospheric limb (focused on providing ozone profile retrievals with higher vertical resolution than is possible from the nadir direction). The nadir mapper has 2800 km instantaneous coverage at the Earth's surface, which is sufficient to provide daily full global coverage at the equator for the NM sensor. For more specifications, consult https://ozoneaq.gsfc.nasa.gov/media/docs/NMTO3-L2_Product_Description.pdf

v. SAGE III: UV/VIS/NIR/SWIR (290-1550 nm) 9-band grating spectrometer with a spectral resolution from 1 to 2 nm. For more

specification, consult https://www.wmo-sat.info/oscar/instruments/view/693.

vi. TES: employs both the natural thermal emission of the surface and atmosphere and reflected sunlight, thereby providing day-night coverage anywhere on the globe. It has significantly more the spectral resolution of the AIRS instrument being flown aboard EOS Aqua. For more specification, consult https://aura.gsfc.nasa.gov/tes.html.

V. Sounder: measures vertical distributions of atmospheric parameters such as temperature, pressure, and composition from multispectral information.

i. MLS: measures naturally-occurring microwave thermal emission from the limb (edge) of Earth's atmosphere. It scans its view from the ground to ~90 km every ~25 seconds 24 hours a day. For more specifications, consult https://mls.jpl.nasa.gov/eos/instrument.php.

ii. AIRS: contains 2378 infrared channels and four visible/near-infrared channels, aimed at obtaining highly accurate temperature profiles within the atmosphere plus a variety of additional Earth/atmosphere products. For more specifications, consult https://aqua.nasa.gov/content/airs.